

JEANS ANALYSIS OF THE GALACTIC THICK DISK AND THE LOCAL DARK MATTER DENSITY

F. J. SÁNCHEZ-SALCEDO¹, CHRIS FLYNN² AND J. A. DE DIEGO¹*Draft version March 29, 2022*

ABSTRACT

Dynamical estimates of the mass surface density at the solar radius can be made up to a height of 4 kpc using thick disk stars as tracers of the potential. We investigate why different Jeans estimators of the local surface density lead to puzzling and conflicting results. Using the Jeans equations, we compute the vertical (F_z) and radial (F_R) components of the gravitational force, as well as $\Gamma(z)$, defined as $\Gamma \equiv \partial V_c^2 / \partial R$, with $V_c^2 \equiv -RF_R$. If we assume that the thick disk does not flare and that all the components of the velocity dispersion tensor of the thick disk have a uniform radial scalelength of 3.5 kpc, Γ takes implausibly large negative values, when using the currently available kinematical data of the thick disk. This implies that the input parameters or the model assumptions must be revised. We have explored, using a simulated thick disk, the impact of the assumption that the scale lengths of the density and velocity dispersions do not depend on the vertical height z above the midplane. In the lack of any information about how these scale radii depend on z , we define a different strategy. By using a parameterized Galactic potential, we find that acceptable fits to F_z , F_R and Γ are obtained for a flaring thick disk and a spherical dark matter halo with a local density $\gtrsim 0.0064 M_\odot \text{pc}^{-3}$. Disk-like dark matter distributions might be also compatible with the current data of the thick disk. A precise measurement of Γ at the midplane could be very useful to discriminate between models.

Subject headings: Galaxy: kinematics and dynamics — Galaxy: solar neighborhood — dark matter

1. INTRODUCTION

It is now generally accepted that our Galaxy contains a dark matter (DM) halo with a virial mass between $0.6 \times 10^{12} M_\odot$ and $3 \times 10^{12} M_\odot$ (e.g., Wang et al. 2015 and references therein). A wide range of experiments are currently ongoing or are planned aiming to detect DM particles by direct scattering between DM and nuclei in detectors or indirectly by their emission of secondary particles from DM annihilations (e.g., Bernabei et al. 2010; Angloher et al. 2012; Aalseth et al. 2013; Agnese et al. 2013; Aartsen et al. 2015). Since the probability of collisions between DM particles and detectors depends on the flux of DM particles, i.e. on the phase-space density, it is crucial to infer the distribution function of DM particles in the Solar system to estimate the chances of direct detection. Based on the disk rotation curve and assuming that DM particles are distributed in a quasi-spherical halo, one infers a typical DM density of $\sim 0.01 M_\odot \text{pc}^{-3}$ at the solar position, and a (one-dimensional) velocity dispersion of $\sim 150 \text{ km s}^{-1}$. However, the density structure of the halo could be more complex: Adiabatic response of the dark halo to the baryonic component or the capture of satellite halos in low-inclination orbits could lead to the formation of a thick dark disk superimposed on the quasi-spherical halo (Read et al. 2008, 2009; Pillepich et al. 2014; Ruchti et al. 2014; Piffl et al. 2015). A dark disk may enhance direct detection because the flux of particles is proportional to the density. If the dark disk is in counter-rotation, the flux is enhanced due to a larger relative velocity between the Sun and the DM particles.

In recent years, many attempts have been carried out to determine the local DM density within a few hundred parsecs of the Sun (see Read 2014 for a review). Several authors have combined data from a wide range of tracers, including the HI rotation curve, and determined the local DM density ρ_0 by fitting a global model for the Milky Way (Catena & Ullio 2010; Weber & de Boer 2010; Iocco et al. 2011; McMillan 2011; Piffl et al. 2014). All these studies are consistent with ρ_0 between 0.005 and $0.015 M_\odot \text{pc}^{-3}$ within 1σ . Other groups have derived ρ_0 , independently of the rotation curve, calculating the gravitational potential up to a height of $1 - 1.5$ kpc, from an equilibrium distribution of tracer stars in the solar neighborhood. From the kinematics of K stars, Garbari et al. (2012) derived a density of $0.022 \pm_{0.013}^{0.014} M_\odot \text{pc}^{-3}$. Zhang et al. (2013), using K dwarfs, measured $\rho_0 = 0.0065 \pm 0.0023 M_\odot \text{pc}^{-3}$. Values of $\rho_0 = 0.008 \pm 0.0025 M_\odot \text{pc}^{-3}$ were derived in Bovy & Rix (2013) by modeling the dynamics of G-type dwarfs. Bienaymé et al. (2014) using red clump stars up to a height of 2 kpc, derived $\rho_0 = 0.0143 \pm 0.0011 M_\odot \text{pc}^{-3}$. In most cases, the results for ρ_0 overlap within their stated uncertainties. Only the 1σ interval of the recent measurement of Bienaymé et al. (2014) does not overlap; if the quoted error bars are not underestimated, this may suggest the existence of potential sources of systematics.

The contribution of the dark halo should clearly manifest at large heights from the midplane. However, Moni Bidin et al. (2010, 2012b) carried out a Jeans analysis of a sample of thick disk stars up to a height of 4 kpc and found no need for DM to account for the observations ($\rho_0 = 0 \pm 0.001 M_\odot \text{pc}^{-3}$). Bovy & Tremaine (2012) re-analysed their data using other model assumptions, finding values fully consistent with standard estimates of this quantity. The estimate of ρ_0 depends on the adopted ra-

¹ Instituto de Astronomía, Universidad Nacional Autónoma de México, Ciudad Universitaria, 04510 Mexico City, Mexico; jsanchez@astro.unam.mx

² Centre for Astrophysics and Supercomputing, Swinburne University of Technology, Australia

dial and vertical scalelengths of the thick disk, denoted by h_R and h_z , respectively. In particular, for $h_R = 2$ kpc and $h_z = 0.7$ kpc, Bovy & Tremaine (2012) obtained $\rho_0 \geq 0.0095 \pm 0.0015 M_\odot \text{pc}^{-3}$, whereas for $h_R = 3.8$ kpc and $h_z = 0.9$ kpc, they found $\rho_0 \geq 0.007 \pm 0.001 M_\odot \text{pc}^{-3}$. More recently, Moni Bidin et al. (2015) have reconsidered their three-dimensional formalism and have found that $\rho_0 = 0 \pm 0.002 M_\odot \text{pc}^{-3}$ for $h_R = 2$ kpc and $h_z = 0.7$ kpc and $\rho_0 = 0.002 \pm 0.003 M_\odot \text{pc}^{-3}$ for $h_R = 3.6$ kpc and $h_z = 0.9$ kpc. It is remarkable that, even using the same data, the estimates on the local DM density in Bovy & Tremaine (2012) and Moni Bidin et al. (2015) differ by one order of magnitude for $h_R = 2$ kpc and $h_z = 0.7$ kpc.

In this paper, we examine why the analyses of Bovy & Tremaine (2012) and Moni Bidin et al. (2015) can give different results and explore the impact of uncertainties in each approach. Then, we suggest a more robust alternative to estimate the surface density, which takes into account information of the kinematics in the radial direction.

The paper is organized as follows. In §2, we outline the basis and assumptions behind the Jeans analysis and present the one-dimensional approach used by Bovy & Tremaine (2012) and the three-dimensional formalism advocated by Moni Bidin et al. (2015). In §3, we compare the predictions of these two estimators of the surface density when using the kinematics of thick disk stars. In order to gain physical insight on the different terms and their uncertainties, we compute the vertical and radial components of the gravitational force, as well as the radial term in the Poisson equation, using the Jeans equations, and compare with the values inferred in representative mass models. In §4, we use some mock data from numerical simulations to identify any possible bias in the assumptions. In §5, we calculate the local parameters of the dark halo, using a parametric method, under the assumption that the DM halo is spherically-symmetric within the solar circle. Conclusions are given in §6.

2. SURFACE DENSITY ESTIMATORS

2.1. Jeans analysis and Poisson equation

The kinematics of tracer stars can be used to determine the gravitational potential of an astronomical object. The Jeans equations provide the strength of the components of the gravitational force from the kinematics of tracer stars. For an axisymmetric steady-state disk with mean velocities $\bar{V}_R = \bar{V}_z = 0$ in cylindrical coordinates, the vertical and radial components of the gravitational force are given by:

$$F_z = \frac{1}{\nu} \left[\frac{\partial(\nu\sigma_z^2)}{\partial z} + \frac{\nu\sigma_{Rz}^2}{R} + \frac{\partial(\nu\sigma_{Rz}^2)}{\partial R} \right], \quad (1)$$

and

$$F_R = \frac{1}{\nu} \frac{\partial(\nu\sigma_R^2)}{\partial R} + \frac{1}{\nu} \frac{\partial(\nu\sigma_{Rz}^2)}{\partial z} + \frac{\sigma_R^2 - \sigma_\phi^2 - \bar{V}_\phi^2}{R}, \quad (2)$$

where $\nu(R, z)$ is the volume mass density of the tracer population, $\sigma_{ij}^2 = \bar{V}_i \bar{V}_j - \bar{V}_i \bar{V}_j$ is its velocity dispersion tensor and \bar{V}_ϕ is its mean velocity in the azimuthal direction. To simplify notation, we use $\sigma_i^2 \equiv \sigma_{ii}^2$.

Once F_z and F_R are known, we may estimate the total density of mass (baryonic plus DM) ρ , using the Poisson equation that relates the gradients of the gravitational force to ρ :

$$4\pi G\rho(R, z) = -\frac{\partial F_z}{\partial z} - \frac{1}{R} \frac{\partial}{\partial R}(RF_R). \quad (3)$$

Integration of the above equation between $-Z_1$ and Z_1 leads us to infer the total column density to Z_1 at a given distance R :

$$2\pi G\Sigma(R, Z_1) = S_{F_z} + S_{F_R}, \quad (4)$$

where

$$S_{F_z} \equiv -F_z(R, Z_1), \quad (5)$$

and

$$S_{F_R} \equiv \frac{1}{R} \int_0^{Z_1} \Gamma(R, z) dz, \quad (6)$$

where

$$\Gamma(R, z) \equiv \frac{\partial V_c^2}{\partial R}, \quad (7)$$

and $V_c^2(R, z) \equiv -RF_R$. We will refer to V_c as the “circular velocity”.

We note that whereas S_{F_z} is positive for a centrally condensed distribution of mass, S_{F_R} may in general be either positive or negative. If the mass distribution is very flattened and oblate, such as in a massive disk, S_{F_z} is larger than $|S_{F_R}|$ at small enough z . For the potential created by a point-mass particle, we have $|S_{F_R}| = S_{F_z}$. Finally, we may have $|S_{F_R}| \gtrsim S_{F_z}$ for a mass distribution elongated along the z axis (i.e. prolate distribution).

F_z , F_R and Γ , and thereby S_{F_z} and S_{F_R} , can be written in terms of the density ν , the velocity dispersions σ_{ij}^2 , and their first and second derivatives (see Appendix A for more details). While S_{F_z} is essentially the vertical force at the height of interest (Z_1), the computation of the term S_{F_R} requires knowledge of the R -gradient of V_c^2 from $z = 0$ to $z = Z_1$. Thus, S_{F_R} is in general more uncertain than S_{F_z} because the computation of S_{F_R} involves second order derivatives along the radial direction³. Therefore, using the Poisson equation is the natural path for deriving Σ when having very small errors in the measured quantities $\nu(R, z)$, $\sigma_{ij}^2(R, z)$ and $\bar{V}_\phi(R, z)$ of the tracer population. At low vertical heights and at distances where the rotation velocity curve is nearly flat, it holds that $|S_{F_R}| \ll |S_{F_z}|$ and thus uncertainties on S_{F_R} will have a minimal effect on the surface density estimate.

We consider the stars in the thick disk as our tracer population and assume that its density distribution can be described by

$$\nu \propto \exp\left(-\frac{R - R_\odot}{h_R} - \frac{|z|}{h_z}\right), \quad (8)$$

where h_R and h_z are the radial and vertical scalelengths, respectively (Siegel et al. 2002; Jurić et al. 2008; Bovy & Rix 2013). The simplest case is to assume that the thick disk has uniform (constant) scalelengths. However, in order to include a possible flare of the tracer disk (e.g.,

³ Particularly uncertain is the radial derivative of \bar{V}_ϕ as a function of z , which is necessary to compute S_{F_R} .

Mateu et al. 2011; Polido et al. 2013; López-Corredoira & Molgó 2014; Minchev et al. 2015), h_z may depend on R ; $h_z = h_z(R)$ and denote $\xi \equiv dh_z/dR$. On the other hand, it is likely that the radial scalelength h_R is not strictly constant with z . Here, we consider the generic case that $h_R(z)$.

Regarding the components of the velocity dispersion, σ_{ij}^2 , we assume that they all exponentially decay along R with scalelength $h_{\sigma_{ij}}$ (Lewis & Freeman 1989; Bovy et al. 2012a; Hattori & Gilmore 2015):

$$\sigma_{ij}^2(R, z) = \sigma_{ij}^2(R_\odot, z) \exp\left(-\frac{R - R_\odot}{h_{\sigma_{ij}}(z)}\right). \quad (9)$$

We will refer to h_R , h_z and $h_{\sigma_{ij}}$ as the “geometrical” parameters. Note that the radial scalelengths of the velocity dispersion tensor ($h_{\sigma_{ij}}$) may vary with z .

Under these approximations, the dynamical estimates of F_z and F_R at $R = R_\odot$, which are denoted by F_z^{est} and F_R^{est} , are

$$F_z^{\text{est}} = \frac{\partial \sigma_z^2}{\partial z} - \frac{\sigma_z^2}{h_z} + k_0 \sigma_{Rz}^2, \quad (10)$$

with $k_0 \equiv R^{-1} - h_R^{-1} - h_{\sigma_{Rz}}^{-1} + \xi z h_z^{-2}$ and

$$F_R^{\text{est}} = k'_0 \sigma_R^2 - \frac{1}{R}(\sigma_\phi^2 + \bar{V}_\phi^2) + \frac{\partial \sigma_{Rz}^2}{\partial z} - \frac{\sigma_{Rz}^2}{h_z}, \quad (11)$$

with $k'_0 \equiv R^{-1} - h_R^{-1} - h_{\sigma_R}^{-1} + \xi z h_z^{-2}$.

Under the same assumptions, the radial derivative of V_c^2 at $R = R_\odot$, which is required to compute S_{FR} , is

$$-\Gamma^{\text{est}} = k_1 \sigma_R^2 + \frac{\sigma_\phi^2}{h_{\sigma_\phi}} + k_2 R \left(\pm \frac{\sigma_{Rz}^2}{h_z} - \frac{\partial \sigma_{Rz}^2}{\partial z} \right) + \frac{\xi R}{h_z^2} \sigma_{Rz}^2 - \frac{\partial \bar{V}_\phi^2}{\partial R} \quad (12)$$

where

$$k_1 = \left(1 - \frac{R}{h_{\sigma_R}}\right) k'_0 - \frac{1}{R} - \frac{zR}{h_z^2} \left(\frac{2\xi^2}{h_z} - \frac{d\xi}{dR} \right), \quad (13)$$

and $k_2 = h_{\sigma_{Rz}}^{-1} - R^{-1}$. The plus-minus sign within the parentheses in Equation (12) indicates that the plus sign must be taken when $z > 0$, and the minus sign when $z < 0$.

We stress that Equations (10)-(13) are valid at $R = R_\odot$. We have omitted extra terms of the form

$$(R - R_\odot) \frac{\sigma_{ij}^2}{h_{\sigma_{ij}}^2} \frac{\partial h_{\sigma_{ij}}}{\partial z}, \quad (14)$$

because we are only interested in the vertical profiles of F_z , F_R and Γ at the cylindrical galactocentric radius of the Sun. At $R \neq R_\odot$, these terms should be taken into account.

2.2. Bovy & Tremaine’s estimator

Bovy & Tremaine (2012) explored the magnitude of S_{FR} for three mass distributions: a single exponential disk with a scalelength of 3.4 kpc, a single NFW halo, and a combination of the two in which the circular speed is flat at R_\odot . They found that $0 \leq S_{FR} \leq 0.2 S_{F_z}$ within $|z| \leq 4$ kpc and suggested, from Equation (4), that the formula

$$\Sigma_{BT}(Z_1) = -\frac{F_z^{\text{est}}(Z_1)}{2\pi G}, \quad (15)$$

with F_z^{est} given in Equation (10) with $\xi = 0$, leads to an underestimate of the surface density to 4 kpc only by $\sim 20\%$. We will refer to this formula as the Bovy & Tremaine (BT) estimator. Note that, unlike the classical one-dimensional approximation (e.g., Read 2014), the cross term of the velocity dispersion, $k_0 \sigma_{Rz}^2$, is included in the computation of F_z^{est} .

Moni Bidin et al. (2015) warned that it may be misleading to assume that $S_{FR}(z)$ is positive for any Galactic mass model, since it depends on the relative weight of the different mass components of the Milky Way. If so, the BT estimator does not necessarily yields a lower limit to the surface density, nor is it accurate within 20%. According to Moni Bidin et al. (2015), the assumption $S_{FR}(z) > 0$ is not adequate to derive ρ_0 because it is implicitly constraining the mass distribution.

2.3. Moni Bidin et al.’s estimator

To compute $\Sigma(Z_1)$, Moni Bidin et al. (2015) prefer to retain the term S_{FR} in Equation (4), and assume that all the geometrical parameters of the thick disk are constant (i.e. the disk does not flare and the scalelengths h_R and $h_{\sigma_{ij}}$ are independent of z). In such a case and combining Equations (6) and (12), we obtain:

$$\Sigma(Z_1) = \frac{1}{2\pi G} (-F_z^{\text{est}}(Z_1) + S_{FR}(Z_1)), \quad (16)$$

where

$$S_{FR}(Z_1) = -\frac{k_1}{R} \int_0^{Z_1} \sigma_{Rz}^2 dz - \frac{1}{R h_{\sigma_\phi}} \int_0^{Z_1} \sigma_\phi^2 dz \quad (17)$$

$$+ k_2 \left(\sigma_{Rz}^2 - \frac{1}{h_z} \int_0^{Z_1} \sigma_{Rz}^2 dz \right) + \frac{2}{R} \int_0^{Z_1} \bar{V}_\phi \frac{\partial \bar{V}_\phi}{\partial R} dz.$$

All the terms in Eq. (17) coincide with those in the equation used in Moni Bidin et al. (2015) –their equation (11)– except the term:

$$- \frac{k_2}{h_z} \int_0^{Z_1} \sigma_{Rz}^2 dz, \quad (18)$$

which does not appear in the equation for Σ used by Moni Bidin et al. (2015). This term will be included in the present study. In fact, we will show in §3.2 that this term may be important for some choices of the geometrical parameters. We will refer to Equation (16) together with Equation (17) as the corrected Moni Bidin et al. (cMB) estimator, which it will be denoted by Σ_{cMB} .

3. APPLICATION TO THE MILKY WAY

3.1. The tracer population: Data and fits

In this Section, we compile the data used to study the different estimators of the local surface density in the Milky Way. As the tracer population, we use the Galactic thick disk. Measurements of the velocity dispersions of 412 thick disk stars were provided by Moni Bidin et al. (2012a). The observed velocity dispersion components of stars, at $|z| > 1.5$ kpc, in the thick disk are:

$$\sigma_R = (82.9 \pm 3.2) + (6.3 \pm 1.1)(|z| - 2.5) \text{ km s}^{-1}, \quad (19)$$

$$\sigma_\phi = (62.2 \pm 3.1) + (4.1 \pm 1.0)(|z| - 2.5) \text{ km s}^{-1}, \quad (20)$$

$$\sigma_z = (40.6 \pm 0.8) + (2.7 \pm 0.3)(|z| - 2.5) \text{ km s}^{-1}, \quad (21)$$

(Moni Bidin et al. 2012a). The vertical profile of the cross term σ_{Rz}^2 is very irregular at $z < 4.5$ kpc. Moni Bidin et al. (2010) fit it by a linear function at $z > 3$ kpc for which they obtained

$$\sigma_{Rz,1}^2 = (1522 \pm 100) + (366 \pm 30)(z - 2.5) \text{ km}^2 \text{ s}^{-2}. \quad (22)$$

This fit was used by Moni Bidin et al. (2012b, 2015) to make a dynamical inference of $\Sigma(z)$. Since all the substructure in σ_{Rz}^2 is well resolved, we include all the data points. Fitting all the available data, we find, for $z > 1.5$ kpc,

$$\sigma_{Rz,2}^2 = (0 \pm 100) + (450 \pm 60)z \text{ km}^2 \text{ s}^{-2}. \quad (23)$$

To apply the cMB estimator, we also need \bar{V}_ϕ and $\partial\bar{V}_\phi/\partial R$. We use

$$\bar{V}_\phi = V_{c,0} - (22.5 \pm 3) - (22.5 \pm 3)|z|^{1.23 \pm 0.03}, \quad (24)$$

where $V_{c,0}$ is the rotational velocity in the midplane at R_\odot , z is given in kpc and \bar{V}_ϕ in km s^{-1} (Moni Bidin et al. 2012a). The adopted values for $V_{c,0}$ will be specified later on. Finally, for $\partial\bar{V}_\phi/\partial R$, we have fitted the data collected by Moni Bidin et al. (2015) from the Sloan Digital Sky Survey (SDSS, York et al. 2000) and the data of Casetti-Dinescu et al. (2011), through a linear function. We obtained

$$\frac{\partial\bar{V}_\phi}{\partial R} = (4 \pm 1)|z| + (1.4 \pm 1.4). \quad (25)$$

Current measurements of $\partial\bar{V}_\phi/\partial R$ are limited to $z \leq 2.7$ kpc. Strictly speaking, the inferences using the above fit for $\partial\bar{V}_\phi/\partial R$ are only valid at $z < 2.7$ kpc.

In their analysis to derive the velocity dispersions of the thick disk stars (Eqs. 19-23), Moni Bidin et al. (2012a) did not account for Poisson noise, which is important due to the small size of the sample. For this reason, Sanders (2012) pointed out that Moni Bidin et al. (2012a) underestimated the gradients of the velocity dispersions with Galactic height. Moni Bidin et al. (2015) argue that the gradient estimates quoted in Moni Bidin et al. (2012a) should be accurate within 15% and that, even enhancing the vertical gradients by a factor of three, the impact on the results is small. In order to have better inferences of the gradients, better data are clearly necessary (Moni Bidin et al. 2015).

3.2. BT estimator vs cMB estimator

Figure 1 shows the disk surface density derived by using the BT estimator (Σ_{BT}) and by using the cMB estimator (Σ_{cMB}). To facilitate comparison with Moni Bidin et al. (2015), we assume $V_{c,0} = 215 \text{ km s}^{-1}$, $\xi = 0$ and use $\sigma_{Rz,1}^2$, as given in Eq. (22). As already stated in Section 3.1, there are no data for $\partial\bar{V}_\phi/\partial R$ beyond $z = 2.7$ kpc. Therefore, the inferences at $z > 2.7$ kpc, using the extrapolation of $\partial\bar{V}_\phi/\partial R$, are shown just to compare the predictions of the different estimators when the same value for $\partial\bar{V}_\phi/\partial R$ is used in all cases.

The integrals in Equation (17) have lower limit $z = 0$. Since we do not have measurements of the velocity dispersions of our tracer population below a height of

1.5 kpc, Equations (19)-(22) were extrapolated down to $z = 0$. The contribution of the term given in Equation (18) cannot be ignored in general. For instance, for $h_z = 0.9$ kpc and $h_{\sigma_{Rz}} = 3$ kpc, its contribution to Σ_{cMB} is $-44.6 M_\odot \text{ pc}^{-2}$ at $z = 4$ kpc.

In order to show the sensitivity of the surface density estimators to changes in the geometrical parameters of the thick disk, we fix h_z to 0.9 kpc and explore different combinations of h_R and h_σ , where we assumed that $h_{\sigma_R} = h_{\sigma_\phi} = h_{\sigma_{Rz}} \equiv h_\sigma$. Figure 1 indicates that Σ_{cMB} is more sensitive to changes in the geometrical parameters than Σ_{BT} . Whereas $\Sigma_{BT}(4 \text{ kpc})$ varies between $95 M_\odot \text{ pc}^{-2}$ to $130 M_\odot \text{ pc}^{-2}$ for the combinations of parameters explored, $\Sigma_{cMB}(4 \text{ kpc})$ varies between $0 M_\odot \text{ pc}^{-2}$ to $110 M_\odot \text{ pc}^{-2}$. Indeed, Σ_{cMB} strongly depends on h_σ . The most sensitive coefficient to h_σ is k_1 ; for instance, for $h_R = 3.5$ kpc, k_1 is reduced by a factor 7.6 when h_σ is varied from 3 kpc to 5 kpc. The strong dependence of $\Sigma_{cMB}(z)$ on h_σ immediately indicates that we need a good measure of h_σ for the cMB estimator to be useful. If h_σ is fixed to 5 kpc, the cMB estimator is very robust to changes in h_R and it holds that $\Sigma_{BT}(z) \lesssim \Sigma_{cMB}(z)$.

Moni Bidin et al. (2012b) noticed that, assuming $h_\sigma = h_R$, their surface density estimations increased with h_R and concluded that in order to have $\Sigma(4 \text{ kpc}) \gtrsim 100 M_\odot \text{ pc}^{-2}$, as extrapolated from the Galactic rotation curve, the thick disk should have an excessively large scalelength h_R ($h_R \gtrsim 4.7$ kpc). Figure 1 shows that the relevant scale is not h_R but h_σ . Indeed, for $h_\sigma = 5$ kpc, we have $\Sigma_{cMB}(4 \text{ kpc}) \simeq 105 M_\odot \text{ pc}^{-2}$, even if the radial scalelength h_R is relatively short ($h_R \simeq 2$ kpc).

In some cases, specifically for $h_R \leq 2$ kpc and $h_\sigma \leq 3$ kpc, the cMB estimator provides a (unphysical) declining estimate for Σ with z , when using the linear fit given in Eq. (25) for $\partial\bar{V}_\phi/\partial R$. If $\partial\bar{V}_\phi/\partial R$ is larger than predicted by our linear fit, the declining trend of Σ_{cMB} with z , found for those cases, can be alleviated. To illustrate how Σ_{cMB} depends on $\partial\bar{V}_\phi/\partial R$, we also show Σ_{cMB} when using a power-law fit of the form $\partial\bar{V}_\phi/\partial R = 4|z|^{1.5} + 1.4$, which also provides a good fit to the data.

Figure 2 shows the estimates of the surface density for two sets of the geometrical parameters. The first set, named as set I, corresponds to $h_R = 2$ kpc, $h_z = 0.7$ kpc and $h_\sigma = 3.5$ kpc, and it is the set preferred by Bovy & Tremaine (2012). The second set of parameters are $h_R = 3.6$ kpc, $h_z = 0.9$ kpc and $h_\sigma = 3.5$ kpc, and were derived by Jurić et al. (2008). The differences between Σ_{BT} and Σ_{cMB} are remarkable. The mismatch between the values predicted by BT and cMB estimators is larger at high z and for the parameter set I. For both set of geometrical parameters, it holds that $\Sigma_{cMB}(z) < \Sigma_{BT}(z)$. In fact, for the model assumptions and the data compiled in §3.1, $S_{FR}(z) < 0$, and, moreover, S_{FR} is comparable in magnitude to S_{Fz} ; in particular, $|S_{FR}| \simeq 0.5 S_{Fz}$ at $z = 4$ kpc.

It can be seen that $\Sigma_{BT}(z)$ increases linearly with z , implying that the density of the DM halo is approximately constant from $z = 1.5$ kpc to 4 kpc. The mean volume density of DM between $z = 1.5$ kpc and $z = 4$ kpc predicted by the BT estimator is $\bar{\rho}_{\text{dm}} \simeq 0.010 M_\odot \text{ pc}^{-3}$ for set I, and $\bar{\rho}_{\text{dm}} \simeq 0.007 M_\odot \text{ pc}^{-3}$ for set II.

On the contrary, $\Sigma_{cMB}(z)$ hardly increases from $z = 1$ to $z = 3$ kpc (see also Moni Bidin et al. 2015), which

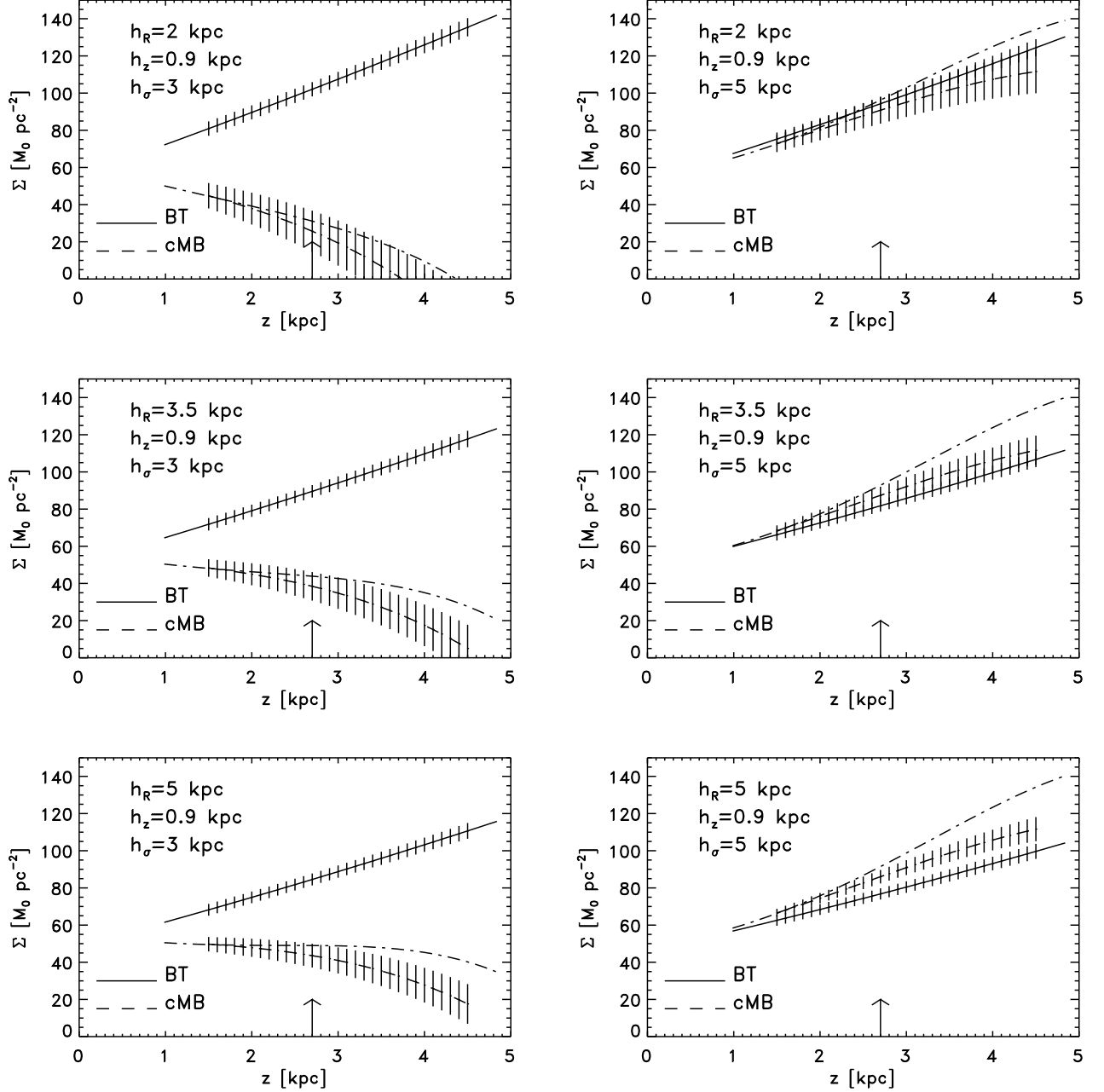


FIG. 1.— Surface density $\Sigma(z)$ predicted in the Milky Way, at $R = R_\odot$, using BT (solid lines) and cMB (dashed lines) estimators for different combinations of the geometrical parameters. In order to evaluate Σ_{cMB} , the observed values of $\partial\bar{V}_\phi/\partial R$ were fit with a linear (dashed lines) and with an $|z|^{1.5}$ -function (dashed-dotted lines). At $|z| > 2.7$ kpc, the values for $\partial\bar{V}_\phi/\partial R$ were extrapolated. The arrows mark this height.

would indicate that the DM density at $|z| > 1$ kpc is small. In fact, since $\rho(z) = (1/2)d\Sigma/dz$, one may conclude that, if Σ_{cMB} is a good estimator and $h_\sigma \leq 3.5$ kpc, then the DM density at $|z| > 1$ kpc is negligible for the parameter set I. Even adopting the most favorable assumptions (parameter set II and the power-law fit for $\partial\bar{V}_\phi/\partial R$), the surface density increases $10M_\odot\text{pc}^{-2}$ from $z = 1$ kpc to $z = 2.5$ kpc, leading to $\bar{\rho}_{\text{dm}} = 0.002 \pm 0.0025 M_\odot\text{pc}^{-3}$ at $|z| > 1$ kpc. The same value was obtained by Moni Bidin et al. (2015). In the next Section, we explore the differences between the predictions of Σ_{BT} and Σ_{cMB} in more detail.

3.3. The gravitational force components and Γ

Figure 3 shows F_z^{est} and F_R^{est} for the parameter sets I and II, using Eqs. (10) and (11). It can be seen that the absolute value of F_z^{est} increases almost linearly with z (that is the reason for the almost linear increase of Σ_{BT} with z). The vertical profile of $|F_R^{\text{est}}|$, on the other hand, is almost flat, with a slight trend to increase with z , particularly for set I. This behaviour of F_R^{est} with z is against expectations because oblate mass distributions predict that $|F_R|$ must decrease with z . This incorrect trend suggests that F_R^{est} is contaminated by systematic

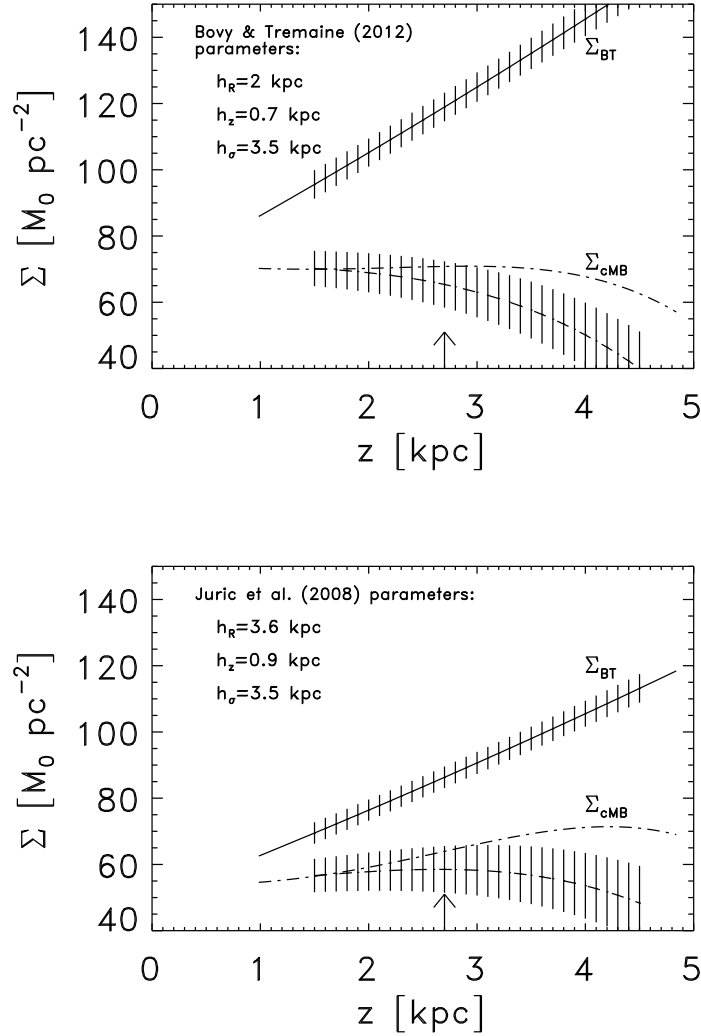


FIG. 2.— Same as Figure 1 but using the parameters of the thick disk preferred by Bovy & Tremaine (2012) –upper panel– and those derived by Jurić et al. (2008) –lower panel–.

uncertainties or poor modeling. Moreover, the values of $|F_R^{\text{est}}|$ are also larger than expected; for the adopted circular velocity of 215 km s^{-1} , F_R at $z = 0$ should be $-V_{c,0}^2/R_\odot = -215^2/8 = -5800 \text{ km}^2 \text{ s}^{-2} \text{ kpc}^{-1}$. Since $|F_R|$ should decrease with z , then $|F_R| \leq 5800 \text{ km}^2 \text{ s}^{-2} \text{ kpc}^{-1}$ at any z . However, $|F_R^{\text{est}}| > 8500 \text{ km}^2 \text{ s}^{-2} \text{ kpc}^{-1}$ for set I and $|F_R^{\text{est}}| > 6500 \text{ km}^2 \text{ s}^{-2} \text{ kpc}^{-1}$ for set II. This also suggests that the adopted value for $V_{c,0}$ is not consistent with the data used to derive F_R^{est} , especially for set I.

The vertical profile for Γ can be derived kinematically using Equation (12), with σ_{ij} , \bar{V}_ϕ and $\partial \bar{V}_\phi / \partial R$ given in §3.1. Note that S_{F_R} is simply the integral of Γ/R over z (see Equation 6). Figure 4 shows that Γ^{est} decreases with z (i.e. $\partial \Gamma^{\text{est}} / \partial z < 0$), acquiring large negative values at $z = 4 \text{ kpc}$. In order to show that this trend for Γ is unphysical, we overplot Γ as a function of z at $R = R_\odot = 8 \text{ kpc}$, for theoretical mass models consisting of a spherically-symmetric component (representing the halo and the bulge), plus a Niyamoto-Nagai

(1975) disk with scalelengths a and b . The spherical component is characterized by the β -parameter defined as $\beta \equiv d \ln V_{\text{tilt}} / d \ln r$, where $V_{\text{tilt}}^2 \equiv r d\Phi_{\text{sph}}/dr$ and Φ_{sph} is the potential associated with the spherical component. The expressions for the R -derivative of V_c^2 are given in the Appendix B.

We explore different relative mass contributions of the disk but in all our models, we have assumed that the circular velocity in the midplane is 215 km s^{-1} , at $R_\odot = 8 \text{ kpc}$. We see that the slope of Γ^{est} vs z cannot be accounted for with a disk and a spherical component; in all the mass models $\partial \Gamma / \partial z > 0$. In spherical models, $\Gamma \geq 0$ at $z > z_{\text{turn}}$, where $z_{\text{turn}} \leq R/\sqrt{2}$ (see Appendix B). In models having a pure disk, $\Gamma > 0$ if $a \geq 4 \text{ kpc}$. Negative values for Γ , as derived from the data (especially for the parameter set I), are very difficult to account for at $z > 2 \text{ kpc}$. In fact, values below $-5000 \text{ km}^2 \text{ s}^{-2} \text{ kpc}^{-1}$ at $z > 2 \text{ kpc}$, as those predicted using the geometrical parameter set I, are not possible even with a very compact mass distribution where all mass were located interior to R_\odot (case $\beta = -0.5$).

TABLE 1
SUMMARY OF THE REPRESENTATIVE MASS MODELS

Model	Dark matter profile	$\bar{\rho}_{\text{dm}}$ $M_{\odot}\text{pc}^{-3}$	$\Sigma(1.5\text{ kpc})$ $M_{\odot}\text{pc}^{-2}$	$\Sigma(4\text{ kpc})$ $M_{\odot}\text{pc}^{-2}$	$V_{c,0}$ km s^{-1}
A	NFW	0.0116	85	143	243
B	NFW	0.0078	71	110	222
C	Thin exp. disk	$\simeq 0.0$	70	70	215
D	Thin exp. disk	$\simeq 0.0$	57	57	215

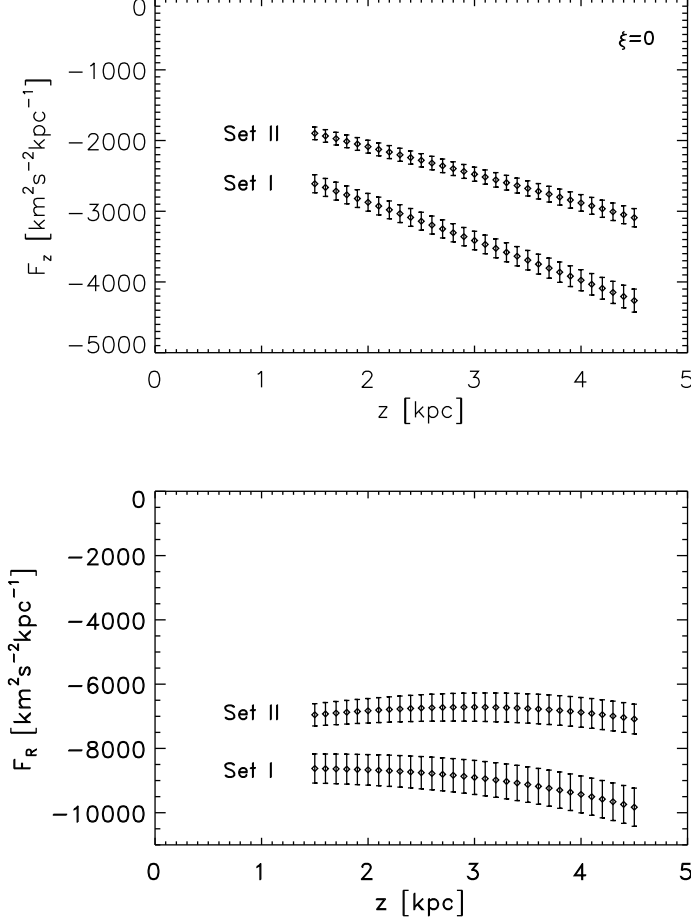


FIG. 3.— Kinematical measurements of the vertical (upper panel) and horizontal (lower panel) components of the gravitational force at R_{\odot} , for set I and set II.

Since the derived values of Γ^{est} are more negative than allowed from generic mass distributions, our first conclusion is that $|S_{F_R}|$ is probably being overestimated and thereby Σ_{cMB} underestimates the surface density in the cases under consideration. It is possible that $|\Gamma^{\text{est}}|$ is being overestimated because (1) either $V_{c,0}$ or $\partial V_{\phi}/\partial R$, or both, have been underestimated, (2) there are heuristics involved in computing the uncertainties in the observed quantities (e.g., Sanders 2012), (3) the mass distribution of the tracer stars cannot be described with a double exponential density profile, (4) the assumptions that the squared velocity dispersions vary all with the same scale length $h_{\sigma_R} = h_{\sigma_{\phi}} = h_{\sigma_{Rz}} = 3.5\text{ kpc}$ and that these scale lengths do not depend on z , are not good approximations, (5) the flaring of the thick disk must be taken into account or (6) a combination of them. Regarding point (4),

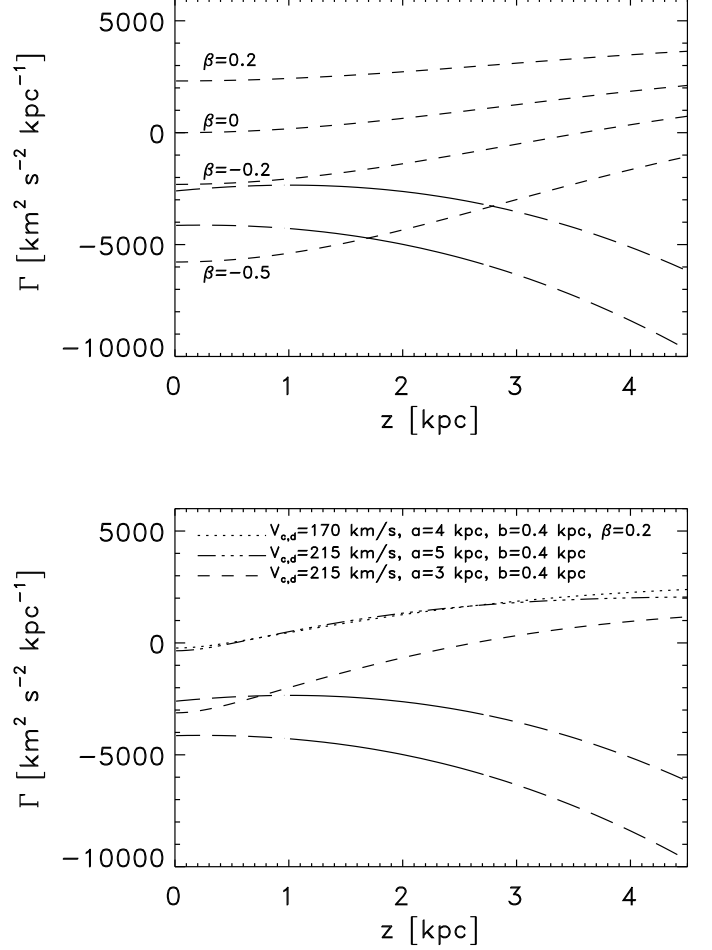


FIG. 4.— Dependence of Γ (the radial derivative of V_c^2), as a function of height. The solid lines represent the Milky Way estimated values using Equation (12) for two sets of parameters: set I (lower solid curve in each panel) and set II (upper solid curve in each panel). The long dashed line indicates that we are using an extrapolation of the linear fit of $\partial V_{\phi}/\partial R$, which was inferred from data at $0.6\text{ kpc} < z < 2.7\text{ kpc}$. Also shown are Γ for several different mass models consisting of a spheroidal component only (upper panel) or a spheroidal component plus a Miyamoto-Nagai disk with parameters a and b (lower panel).

we comment that measurements of the radial scale of the velocity dispersion in the Milky Way are scarce. Lewis & Freeman (1989) measured the radial variation of σ_R^2 and σ_{ϕ}^2 in the plane of the old disk from about 1 to 17 kpc in galactocentric radius and found $h_{\sigma_R} = 4.37 \pm 0.32\text{ kpc}$ and $h_{\sigma_{\phi}} = 3.36 \pm 0.62\text{ kpc}$. The difference between h_{σ_R} and $h_{\sigma_{\phi}}$ was interpreted as suggesting that the rotation curve is not precisely flat in the range of galactocentric distances covered by observations. On the other hand,

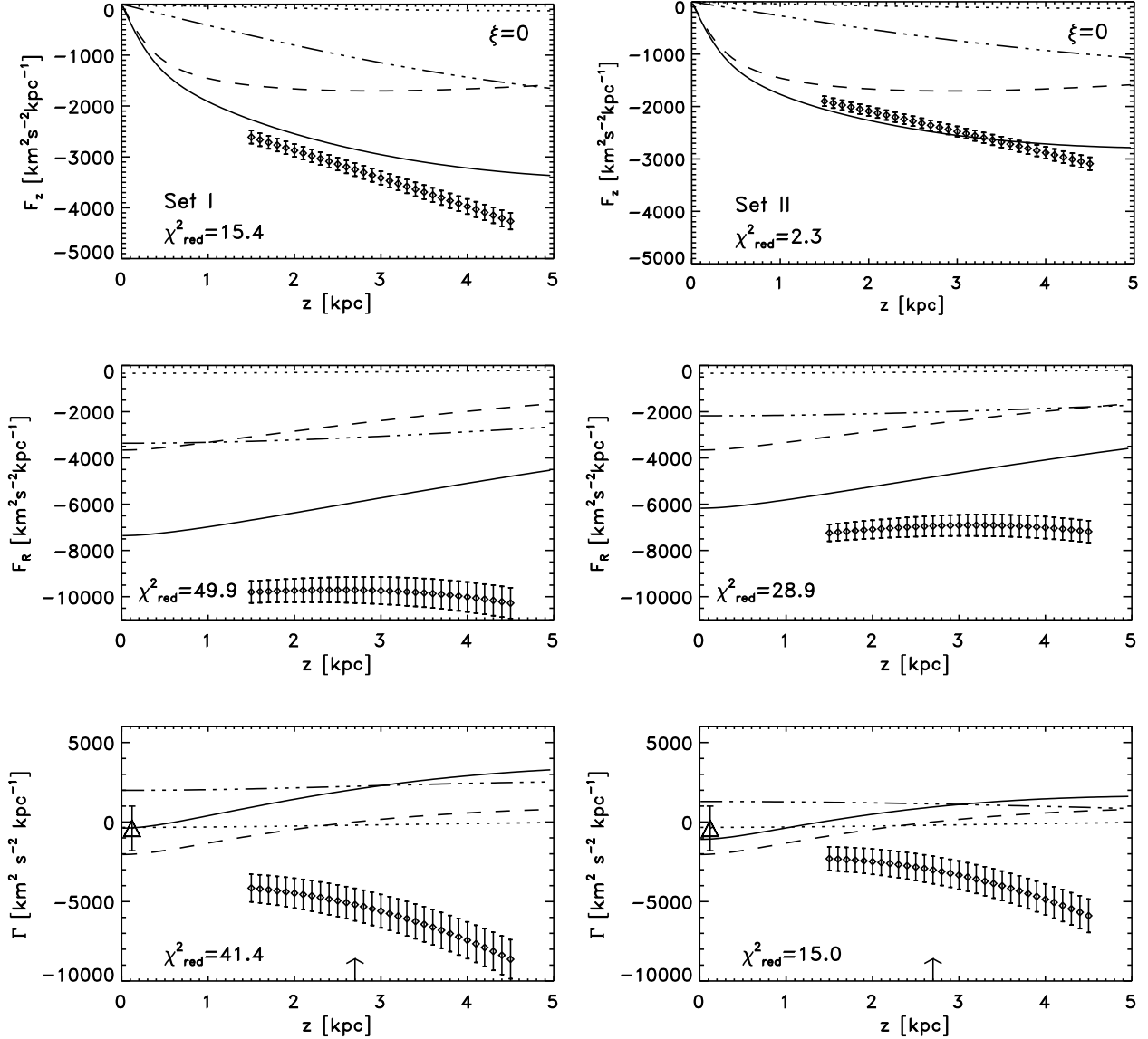


FIG. 5.— Vertical profiles of F_z , F_R and Γ , at R_\odot . The kinematical estimates were derived using Eqs. (10), (11) and (12) (dots with error bars) with the parameters set I (left column) and with set II (right column). The solid line represent the values in the mass model A (left column) and in mass model B (right column). In these models, the DM resides in an NFW halo. For the baryonic mass, we used the model described in §5. The contribution of each component is also shown: the dark component (triple dot-dashed line), visible disk (dashed line) and bulge (dotted line). The triangle with the bar indicates the interval of values derived using recent determinations of the Oort constants (see Table 2). The arrows at the bottom panels remind the reader that we have extrapolated the observed values of $\partial\tilde{V}_\phi/\partial R$ at heights > 2.7 kpc. The quoted value of χ^2_{red} for Γ was computed within $1.5 < z < 2.7$ kpc.

the radial scale of σ_z was found to be 3.5 kpc by (Bovy et al. 2012a) and 4.1 ± 1 kpc by Hattori & Gilmore (2015). Therefore, there is no reason to assume that all the components of the velocity dispersion tensor have the same scale lengths.

In an attempt to assess the reliability of the dynamical estimates of the local surface density and to check if their unexpected too low values were an artifact of the assumed kinematics, Moni Bidin et al. (2012b) repeated the calculations using two independent data sets for the kinematics of the thick disk stars. It is remarkable that the three sets returned similar values for the surface density. This might indicate that either all data sets are affected by the same systematics, or the model assump-

tions are not adequate (or both). In the next Sections, we will try to shed light on these issues.

3.4. Representative mass models

In the previous subsection, we showed that both F_R^{est} and Γ^{est} take values more negative than expected if $V_{c,0} = 215 \text{ km s}^{-1}$. It is worthwhile to calculate F_z , F_R and Γ in simple global mass models and compare them with the values derived as using the kinematical data of the thick disk. To do so, we consider four representative mass models, referred as models A, B, C and D. A summary of the relevant parameters of each model is given in Table 1. We also give $\bar{\rho}_{\text{dm}}$ which represents the mean volume density of DM between $z = 1.5$ kpc and $z = 4$

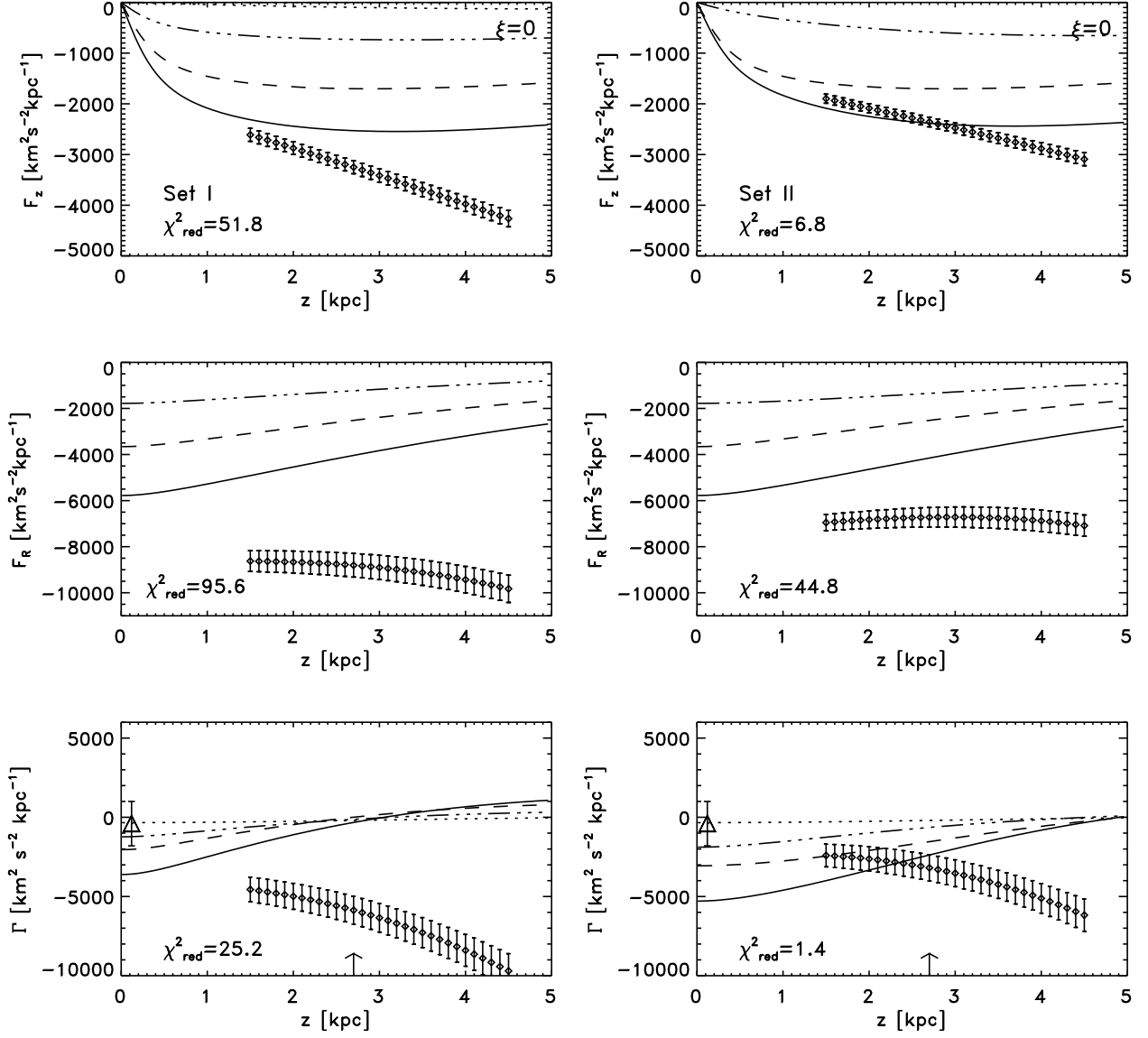


FIG. 6.— Same as Figure 5 but for models C (left column) and D (right column). In these models the DM resides in a thin exponential disk. The radial scale lengths of the DM disk were chosen in order to have a local circular velocity of 215 km s^{-1} .

kpc. All the mass models have the same distribution of baryonic mass, but differ in the dark matter distribution. The baryonic mass is distributed as follows (see §5.1 for details and references); a bulge of mass $5 \times 10^9 M_\odot$, a radially exponential stellar disk with scalelength 2.15 kpc , and a local surface density of $38 M_\odot \text{ pc}^{-2}$, the ISM layer modeled as a radially exponential disk with a scalelength of 8.5 kpc and a local surface density of $13 M_\odot \text{ pc}^{-2}$.

Models A and B have local surface densities $\Sigma(4 \text{ kpc})$ similar to the values derived using the BT estimator for set I and set II, respectively (see §3.2 and Table 1). For these models, we assume the DM is distributed in a NFW halo with a scale radius of 19 kpc . For this scale radius, the circular velocity at R_\odot is $\sim 220 - 245 \text{ km s}^{-1}$ (see Table 1). In particular, the parameters of the DM halo in model A are similar to those inferred by Nesti & Salucci (2013) to fit the rotation curve of our Galaxy with a NFW profile.

In §3.2, we found that Σ_{CMB} predicts a surface density of $\simeq 70 M_\odot \text{ pc}^{-2}$ at $z = 1.5 \text{ kpc}$ for the set I, and a surface density of $\simeq 57 M_\odot \text{ pc}^{-2}$ for the set II. Thus, assuming that the surface density in visible matter is $\simeq 51 M_\odot \text{ pc}^{-2}$ (eg., Bovy & Rix 2013), Σ_{CMB} would imply that the DM should lie in a thin disk with a scaleheight $\lesssim 1 \text{ kpc}$ and a local surface density $\sim 19 M_\odot \text{ pc}^{-2}$ (parameters set I) and $\sim 6 M_\odot \text{ pc}^{-2}$ (set II). To mimic these density profiles, models C and D assume that there is a DM component, which is deposited in a radially exponential disk with a scaleheight $< 1 \text{ kpc}$ and local surface density of $19 M_\odot \text{ pc}^{-2}$ (model C) and $6 M_\odot \text{ pc}^{-2}$ (model D). The radial scalelength for the DM disk was chosen in order to give a local circular velocity of 215 km s^{-1} , to be consistent with the value adopted in §3.2. More specifically, the radial scalelength for the DM disk is 2.1 kpc for model C and 1.4 kpc for model D.

In Figures 5 and 6, we compare the values of F_z , F_R

and Γ of the models A, B, C and D with the kinematical measurements of these quantities. In order to compare the different models, the reduced chi-square, χ^2_{red} , defined as χ^2/N , where N is the number of data points, are given at each panel. In the case of Γ , the quoted value of χ^2_{red} was calculated using only the data points within $1.5 \text{ kpc} \leq z \leq 2.7 \text{ kpc}$ because there exist direct measurements of $\partial \bar{V}_\phi / \partial R$ only up to $z = 2.7 \text{ kpc}$ (see §3.1).

The linear shape of F_z^{est} cannot be reproduced if all the mass is distributed in a disk (models C and D; see upper panels in Fig. 6). As expected from the analysis in §3.3, all the mass models have $|F_R|$ values that are smaller than $|F_R^{\text{est}}|$. For instance, $|F_R^{\text{est}}|$ at $z = 4 \text{ kpc}$ (calculated using the parameters set I) is a factor of 2–3 larger than it is in the mass models A and C. The fact that both $|F_z^{\text{est}}|$ and $|F_R^{\text{est}}|$ are larger than they are in the mass models A and C, suggests that the data allows a more massive dark component than adopted in these mass models.

On the other hand, the profile of Γ , as derived from the kinematics of the thick disk, is much more negative than in the mass models. The discrepancies in F_R and also in Γ are somewhat mitigated when the parameters set II are used.

From the χ^2 -statistics, there is no any clear preference for model B or for model D. Model B explains better F_z^{est} and F_R^{est} but model D is better in accounting for the large negative values of Γ^{est} between $z = 1.5 \text{ kpc}$ and $z = 2.7 \text{ kpc}$. A remarkable difference between models B and D is the value of Γ_0 , defined as $\Gamma_0 \equiv \Gamma(R_\odot, 0)$. Model B has $\Gamma_0 = -1000 \text{ km}^2 \text{ s}^{-2} \text{ kpc}^{-1}$, whereas Model D has $\Gamma_0 = -5200 \text{ km}^2 \text{ s}^{-2} \text{ kpc}^{-1}$ (see solid lines in the lowest right panels in Figures 5 and 6). Good observational measurements of Γ_0 at $z = 0$ are crucial to discriminate between different models; indeed, very different mass models may have similar values of both F_z and F_R at $0 \leq z \leq 4 \text{ kpc}$.

It is generally assumed that the inner rotation curve is rather flat, typically $\partial \ln V_c / \partial \ln R = 0 \pm 0.15$ at $z = 0$ (e.g., Salucci et al. 2010). The most common way to estimate Γ_0 is via the Oort constants A and B :

$$\Gamma_0 = 2R(B^2 - A^2). \quad (26)$$

For recent values of the Oort constants derived using the proper motion of relatively old giant stars, which are one of the most reliable tracers, we find that Γ_0 lies between -2000 and $1000 \text{ km}^2 \text{ s}^{-2} \text{ kpc}^{-1}$ (see Table 2). From the velocity distribution of stars in the thin-disk population, Fuchs et al. (2009) found that the rotation curve at R_\odot is almost flat ($\partial \ln V_c / \partial \ln R = -0.006 \pm 0.016$ at $z = 0$). Therefore, model B is more in accordance with the observational inferences of Γ_0 .

We have also explored other variants of models C and D. For instance, exponential dark disks having the same local surface density, but a larger radial scalelength (8.5 kpc). In these models, a spherical DM component with null density at $r > R_\odot$, was added to satisfy the condition that $V_{c,0} = 215 \text{ km s}^{-1}$. No significant changes in F_z , F_R or Γ were found in these models as compared to models C and D.

4. TESTS USING NUMERICAL SIMULATIONS

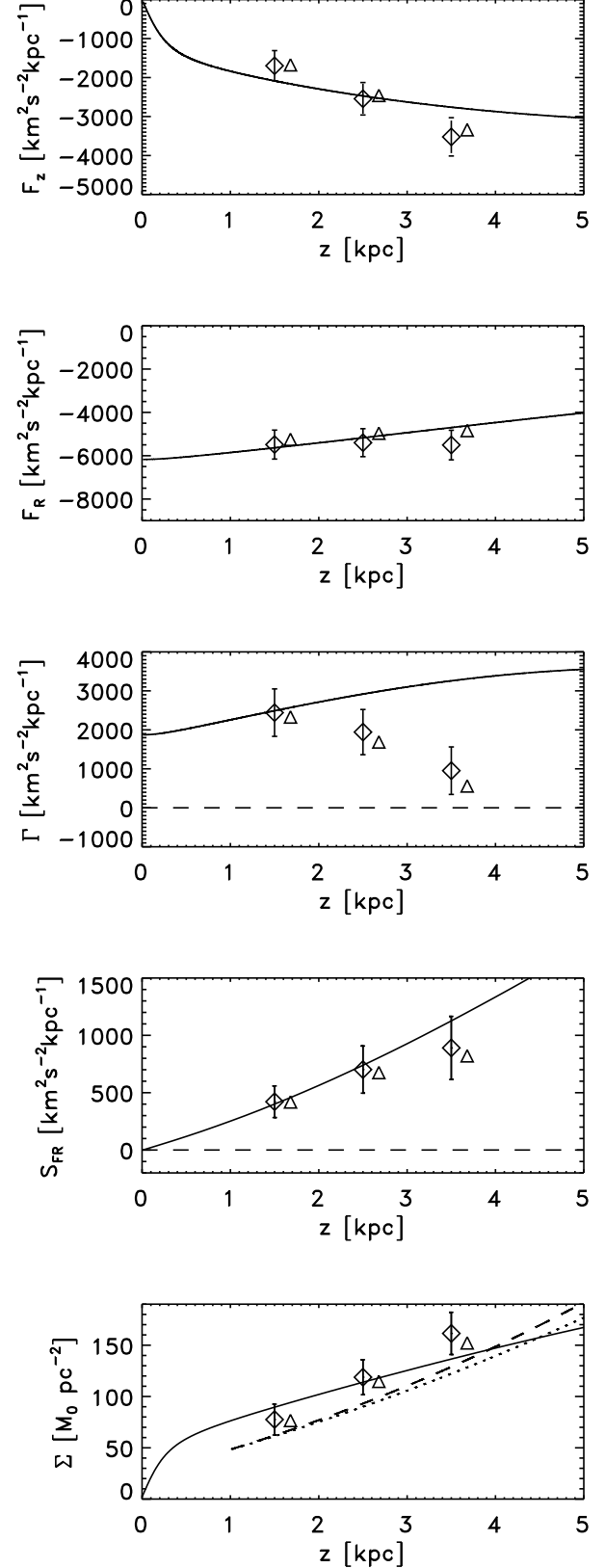


FIG. 7.— Comparison of the exact values of F_z , F_R , Γ , S_{FR} and Σ in our simulations (solid lines), as a function of height, with their corresponding dynamical measurements, using Eqs. (10)–(12) with $\xi = 0$ (triangles) and $\xi = -0.02$ (dots with error bars). To make the plot readable, the triangles have been slightly shifted in the horizontal direction. The dashed lines indicate the values in the BT method. In the last panel, the dashed (dotted) line represents Σ_{BT} for $\xi = -0.02$ ($\xi = 0$) and the dots with error bars are for Σ_{cMB} .

TABLE 2
ESTIMATES OF THE R -DERIVATIVE OF V_c^2 , Γ , AT $z = 0$

Stellar Type	A $\text{km s}^{-1}\text{kpc}^{-1}$	B $\text{km s}^{-1}\text{kpc}^{-1}$	Γ_0 $\text{km}^2 \text{s}^{-2}\text{kpc}^{-1}$	References
Cepheids	14.82 ± 0.84	-12.37 ± 0.64	-1100 ± 500	Feast & Whitelock (1997)
K, M giants	14.5 ± 1.0	-11.5 ± 1.0	-1250 ± 600	Mignard (2000)
K, M giants	15.86 ± 1.30	-14.57 ± 1.01	-650 ± 800	Yuan et al. (2008)
Red giants	9.6 ± 0.5	-11.6 ± 0.5	700 ± 250	Olling & Dehnen (2003)
F giants	14.85 ± 7.47	-10.85 ± 6.83	-1650 ± 4000	Branham (2010)
APOGEE	$13.5^{+0.2}_{-1.0}$	$-13.7^{+3.3}_{-0.1}$	100^{+100}_{-1300}	Bovy et al. (2012b)

In this Section, we measure different quantities (e.g., vertical and radial components of the gravitational force, surface density) using the kinematics of the tracer population in a simulated galaxy, as if it is done for the thick disk of the Milky Way, and then compare them with the exact input values. In particular, we will be able to quantify the role of systematic uncertainties and the impact of the assumptions in the above quantities, particularly, the surface density.

4.1. Our mock galaxy

A thick disk-like tracer population, containing 10^5 stars, was set up in a rigid disk+bulge+dark halo potential. For the gravitational potential, we adopt the analytical model described in Flynn et al. (1996). The model is composed of two spheroidal components (bulge plus a inner core), three Miyamoto-Nagai disks and a spherical dark halo. Given the background potential, the exact input values of S_{F_z} and S_{F_R} can be calculated. Since the rotation curve at the midplane in this model is rising at the solar position, it holds that $S_{F_R} > 0$. At $z > 2.5$ kpc, S_{F_R} is not negligible as compared to S_{F_z} . For instance, $S_{F_R} = 0.4S_{F_z}$ at $z = 3.5$ kpc. As a consequence, Σ_{BT} is expected to underestimate the surface density by $\sim 28\%$. We wish to test the predictions of Σ_{BT} and Σ_{cMB} in a situation where the tracer population is a thick disk with a surface density that decays exponentially with R . In the vertical direction, the volume density is close to exponential as well.

The exponential density scale-height, velocity dispersions and mean rotation rates of the tracer stars were set up initially to match, as closely as we could, the data of Moni Bidin et al. (2012a). Once the disk was relaxed in the rigid background potential of the galaxy, the orbits were integrated for 5 Gyr.

We calculated the velocity dispersions of the stars that are within $7.5 \leq R \leq 8.5$ kpc, at three heights: $z = 1.5, 2.5$ and 3.5 kpc. At $|z| \geq 1.5$ kpc, the velocity dispersions were fitted well by:

$$\sigma_R = (72 \pm 3) + (3.2 \pm 1)(|z| - 2.5) \text{ km s}^{-1}, \quad (27)$$

$$\sigma_\phi = (61 \pm 3) + (2.7 \pm 1)(|z| - 2.5) \text{ km s}^{-1}, \quad (28)$$

$$\sigma_z = (45 \pm 3) + (6 \pm 1)(|z| - 2.5) \text{ km s}^{-1}. \quad (29)$$

The antisymmetric velocity dispersion component σ_{Rz}^2 was fitted by

$$\sigma_{Rz}^2 = (1000 \pm 450) + (550 \pm 150)(z - 2.5) \text{ km}^2 \text{ s}^{-2}. \quad (30)$$

The latter expression holds for $z > 1.5$ kpc. We note that the values of σ_{Rz}^2 are somewhat smaller in our simulations than the observed values reported in Moni Bidin et al. (2010).

The mean azimuthal velocity \bar{V}_ϕ , at $R = 8$ kpc, was fit between $z = 0.5$ to $z = 4$ kpc using $\bar{V}_\phi = 197 - 20|z|^{1.3} \text{ km s}^{-1}$ (with z in kpc). The fit is good and has residuals of less than 4 km s^{-1} . It is remarkable that a similar z -dependence for $\bar{V}_\phi(z)$ was found for thick disk stars by Ivezić et al. (2008) from the analysis of SDSS data, and by Moni Bidin et al. (2012a) combining different data sets. Finally, we also computed $\partial \bar{V}_\phi / \partial R$ at $R = 8$ kpc, from the simulations, and found $\partial \bar{V}_\phi / \partial R = 2.8|z| + 5.5 \text{ km s}^{-1} \text{ kpc}^{-1}$ (with z in kpc). The residuals are less than $0.6 \text{ km s}^{-1} \text{ kpc}^{-1}$.

4.2. Dynamical tests

The vertical profiles of F_z , F_R , Γ , Σ_{BT} and Σ_{cMB} can be derived from the kinematics of the tracer population using Equations (10)-(16) and compare them with the input values. The z -derivatives of the velocity dispersions in Equations (10)-(12) and the integrals over z in Equation (17) were performed analytically using the linear fits given in Equations (27)-(30). In the computation of S_{F_R} and Σ_{cMB} , we used $z = 0$ as the lower limit of integration in Equation (17) as we did in §3.2.

In principle, the geometrical parameters of the simulated thick disk can be measured from our simulations. However, they are not constant with height, but depend on z . In order to quantify the impact of the assumption that the geometrical parameters are constant, we have computed F_z^{est} , F_R^{est} , Γ^{est} , $S_{F_R}^{\text{est}}$, Σ_{BT} and Σ_{cMB} using the mean geometrical parameters. We have measured the *mean* geometrical parameters in our simulations, which will be denoted by an asterisk, by computing the velocity dispersion tensor vs R in the range $4 < R < 12$ kpc, including all the stars within $|z| < 2.5$ kpc. We obtained $h_z^* = 0.77$ kpc, $h_R^* = 4.0$ kpc, $h_{\sigma_R}^* = 5.5$ kpc, $h_{\sigma_\phi}^* = 4.6$ kpc and $h_{\sigma_{Rz}}^* = 4.1$ kpc. Figure 7 shows F_z^{est} , F_R^{est} , Γ^{est} , $S_{F_R}^{\text{est}}$, Σ_{BT} and Σ_{cMB} , derived using the mean geometrical parameters and the *exact value* of $V_{c,0}$. Although our simulated thick disk exhibits a slight “antiflaring” with $\xi^* = -0.02$ at R_\odot , we show results for both $\xi = -0.02$ and $\xi = 0$.

It can be seen that the dynamical measurement of F_z overestimates the modulus of the vertical force beyond $z = 2.5$ kpc and underestimates it below this height. In other words, the slope of F_z versus z is not well reproduced by the kinematical estimates, but the mean value of F_z between $z = 1.5$ kpc and $z = 3.5$ kpc is estimated correctly. The effect of using either $\xi = 0$ or $\xi = -0.02$ is small.

The R -component of the force is well reproduced, particularly for $\xi = 0$. The shape of F_R^{est} vs z is slightly flatter than the input simulation values for $\xi = -0.02$.

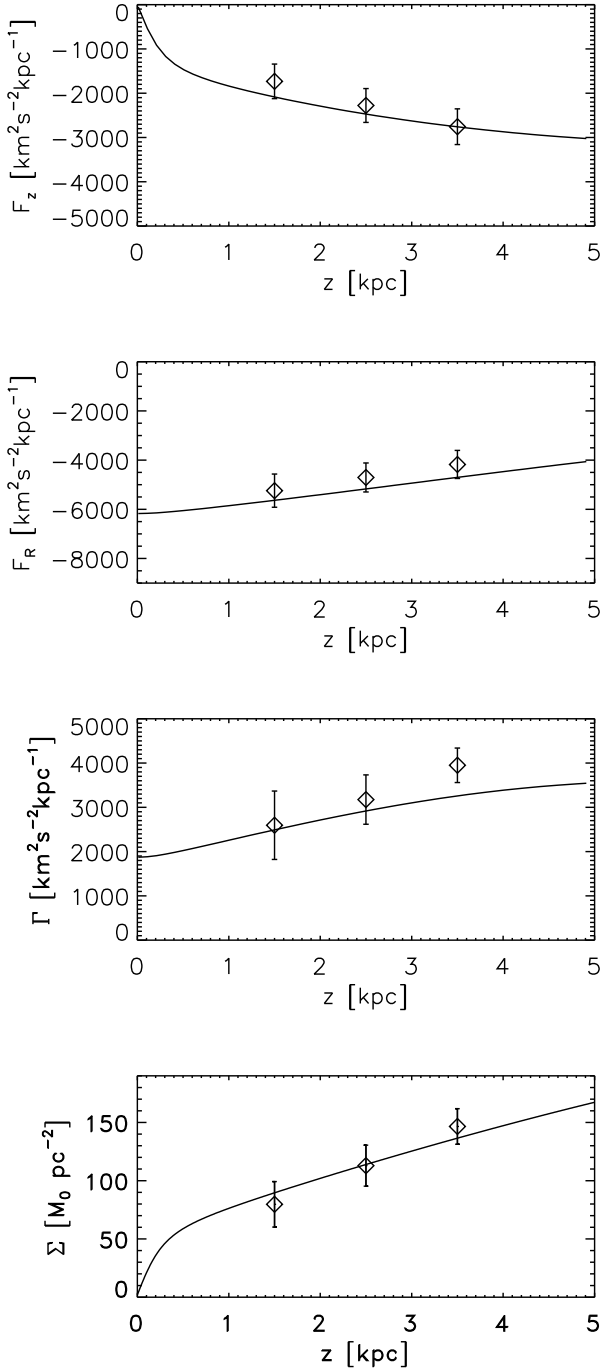


FIG. 8.— Dynamical measurements of F_z , F_R , Γ and Σ at $R = 8$ kpc from our simulations using the generalized Equations given in Appendix A, which depend on the local values of the geometrical parameters, as they vary with z (dots with error bars). For comparison, we show also their exact vertical profiles (solid lines).

On the other hand, the dynamical inferences of Γ deviate significantly from the real input values at $z > 2.5$ kpc. S_{F_R} is underestimated as well, but since S_{F_R} is an integral of Γ over z , S_{F_R} presents a smaller fractional error than Γ .

As expected, Σ_{BT} underestimates the surface density because of the assumption $S_{F_R} = 0$. However, the difference between the real and the predicted value at $z = 3.5$

kpc is only $10 - 15 M_\odot \text{ pc}^{-2}$, that is $\sim 8.5\%$ (much less than the expected value of 28%; see Section 4.1). The reason is that S_{F_z} is overestimated and this compensates the ignored positive contribution of S_{F_R} .

Σ_{cMB} reproduces the surface density within the uncertainties. At $z = 3.5$ kpc, the value predicted for $\xi = 0$ is closer to the exact value. Both estimators equally overestimate S_{F_z} , but Σ_{BT} compensates it by adopting $S_{F_R} = 0$ and Σ_{cMB} does not. Note that both estimators overpredict the slope of Σ with z , mainly because F_z^{est} is steeper than the real profile.

As already anticipated, the geometrical parameters depend on z . In our particular simulation, we have measured the local geometrical parameters \tilde{h}_z , \tilde{h}_R and $\tilde{h}_{\sigma_{ij}}$ (see Appendix A for their definitions) and found they increase with z , except h_R . For instance, \tilde{h}_z increases from 0.76 kpc at $z = 1.5$ kpc to 0.91 kpc at $z = 3.5$ kpc, and \tilde{h}_R decreases from 3.8 to 3.0 kpc in the same range. The changes of $\tilde{h}_{\sigma_{ij}}$ are more remarkable: \tilde{h}_{σ_R} varies from 6.0 kpc at $z = 1.5$ kpc, to $\gtrsim 25$ kpc at $z = 3.5$ kpc (\tilde{h}_{σ_ϕ} varies by a factor of 2.5 and $\tilde{h}_{\sigma_{Rz}}$ by a factor of 1.8). Figure 8 shows that when the local scalelengths are used at each z (see Appendix A), all the values are recovered within the uncertainties, except the value of Γ at $z = 3.5$ kpc. Note that the error bars in Figure 8 do not include uncertainties in the measured geometrical parameters. In particular, the second-order R -derivatives involved in the computation of Γ may introduce significant bias (see Appendix A).

In our particular thick disk realization, Σ_{cMB} overestimates Σ at $z = 3.5$ kpc because h_z increases with z . Were h_z nearly constant in the region of interest, Σ_{cMB} would have predicted correctly the surface density. The two estimators should be mutually consistent if the selected stars represent a homogenous population with constant geometrical parameters and the underlying potential is such that S_{F_R} is small as compared to S_{F_z} . If the geometrical parameters were constant but S_{F_R} cannot be ignored as compared to S_{F_z} , Σ_{cMB} is a more reliable estimator. In the lack of any information about the vertical dependence of the geometrical parameters, it is not possible to discern what estimator is more reliable.

So far, we have assumed that we know the mean geometrical parameters with enough accuracy. In real life, uncertainties in the mean values of the geometrical parameters of the thick disk are large. In order to test the robustness of the dynamical estimates to these uncertainties, we have repeated the calculation assuming $h_{\sigma_R} = h_{\sigma_\phi} = h_{\sigma_{Rz}} = 3.5$ kpc, instead of the exact values. In this case, F_z^{est} and F_R^{est} are almost unaltered by the new choice of the geometrical parameters. However, the new parameters clearly underestimates S_{F_R} , which becomes close to zero; thus $\Sigma_{cMB} \simeq \Sigma_{BT}$. Therefore, in this case, both predictors give similar results.

5. THE PARAMETRIC METHOD

5.1. Description of the method

According to §4, if the selected stars represent a homogeneous population, that is not formed by mixing of populations with different scalelengths, and if the mean geometrical parameters and $V_{c,0}$, \bar{V}_ϕ and $\partial \bar{V}_\phi / \partial R$ are known with good precision, S_{F_R} is recovered within the

uncertainties. However, in §3.3 we found that S_{FR} takes implausibly large negative values when calculated using the currently available kinematical data of the thick disk. Therefore, uncertain input parameters, systematic uncertainties or/and incomplete modeling are possibly contaminating S_{FR} .

An alternative means of estimating the surface density Σ is to fit a parameterized galaxy potential to F_z^{est} , F_R^{est} and Γ^{est} . Once the best-fitting parameters are found, $\Sigma(z)$ can be computed. We will refer to this as the *parametric method*. This method provides physically meaningful solutions and it also includes information of the radial force field, which is in the spirit of three-dimensional approaches.

We use a simplified model for the Milky Way composed by a bulge, a disk and a dark halo. To reduce the number of free parameters of the model and to avoid large levels of degeneracy between parameters, we fix the parameters of the visible matter and allow to vary the parameters of the dark halo. At $r \geq R_\odot$, the stellar bulge is modeled as a potential $\Phi_b \simeq -GM_b/r$, with a mass M_b of $5 \times 10^9 M_\odot$ (e.g., McMillan 2011). For the local surface density of the stellar disk, we take $38 M_\odot \text{ pc}^{-2}$ (Bovy & Rix 2013). Bovy & Rix (2013) presented a dynamical measurement of the mass-weighted Galactic disk scale length R_d , using the kinematics of abundance-selected stellar populations from the SEGUE survey. They found $R_d = 2.15 \pm 0.14$ kpc. Since we wish to explore models as consistent as possible with the dynamical constraints derived in Bovy & Rix (2013), we have fixed the mass-weighted scalelength of the disk to $R_d = 2.15$ kpc, and the mass scale height to 0.37 kpc (Bovy & Rix 2013). To derive the gravitational forces created by the stellar disk, it was approximated with three Miyamoto-Nagai potentials with the expressions in Smith et al. (2015), which provide a good approximation for the potential created by an exponential disk. The mass distribution of the ISM layer was represented by an exponential disk with a local surface density of $13 M_\odot \text{ pc}^{-2}$ (Holmberg & Flynn 2000), and a long radial scalelength of 8.5 kpc to reproduce the plateau in the gas surface density (e.g., Wolfire et al. 2003). We set the vertical height of the gaseous disk to 0.35 kpc, but its exact value is not relevant for the present study.

As discussed in §3.3 and 3.4, the currently available kinematic data for the thick disk stars alone, are of insufficient quality to uniquely determine the profile of $\Sigma(z)$, without making further assumptions. To break down the degeneracy between models, we here aim at calculating the parameters of the DM halo and the geometrical parameters of the thick disk that better match the data, with the simplistic but restrictive assumption that the DM halo is spherically-symmetric. The dark halo was assumed to have a circular velocity following a power-law with index β_h , $V_h \propto r^{\beta_h}$ in the region of interest, that is between a galactocentric radius $r_1 = R_\odot = 8$ kpc and $r_2 = (R_\odot^2 + z_{\text{max}}^2)^{1/2} \simeq 9.2$ kpc, for $z_{\text{max}} = 4.5$ kpc. The two parameters that characterize the dark halo are the corresponding circular velocity at R_\odot , denoted by $V_{h,\odot}$, and the β_h parameter. We note that we do not force the DM halo to match the expected DM density of any classical model; if there is no need for DM interior to R_\odot to explain the local kinematics of the thick disk,

we should obtain $V_{h,\odot} \simeq 0$. A value for β_h close to the Keplerian value (-0.5) would imply that the kinematics of the thick disk is consistent with a zero local density halo.

Knowing $V_{h,\odot}$ and β_h , we may estimate the mean density of dark matter between r_1 and r_2 as

$$\bar{\rho}_{\text{dm}} = \frac{3}{4\pi} \frac{M_h(r_2) - M_h(r_1)}{r_2^3 - r_1^3}, \quad (31)$$

with $M_h(r)$ the DM mass interior to r :

$$M_h(r) = \frac{r V_h^2(r)}{G} = \left(\frac{r}{R_\odot}\right)^{2\beta_h} \frac{r V_{h,\odot}^2}{G}. \quad (32)$$

The DM density can be estimated as:

$$\rho(r) = \frac{1}{4\pi G r^2} \frac{dM_h}{dr} = (1 + 2\beta_h) \frac{V_h^2(r)}{4\pi G r^2}. \quad (33)$$

In particular, the local DM density is:

$$\rho_0 = (1 + 2\beta_h) \frac{V_{h,\odot}^2}{4\pi G R_\odot^2}. \quad (34)$$

5.2. Results

To estimate F_z^{est} , F_R^{est} and Γ^{est} , we need to set the geometrical parameters of the thick disk. To facilitate comparison with Bovy & Tremaine (2012) and Moni Bidin et al. (2015), we start by considering a model with $h_R = 3.6$ kpc, which corresponds to the scalelength derived by Jurić et al. (2008). They estimated an error in h_R of 20%. As far as we know, the only measurements of h_{σ_R} and h_{σ_ϕ} were provided by Lewis & Freeman (1989). They estimated $h_{\sigma_R} = 4.37 \pm 0.32$ kpc and $h_{\sigma_\phi} = 3.36 \pm 0.62$ kpc (for $R_\odot = 8.5$ kpc and $V_{c,0} = 220 \text{ km s}^{-1}$). For σ_z^2 , Bovy et al. (2012a) found a scalelength of 3.5 kpc, whereas Hattori & Gilmore (2015) derived a value of 4.1 ± 1 kpc. Following Bovy & Rix (2013), we set $h_{\sigma_R} = h_{\sigma_\phi} = 4$ kpc. For $h_{\sigma_{Rz}}$ we adopt a value of 3.5 kpc, similar to the scalelength observed for σ_z by Bovy et al. (2012a).

Values for the flare parameter of the thick disk, ξ , between 0.01 and 0.02 were found by Mateu et al. (2011) and by López-Corredoira & Molgó (2014). Therefore, we perform the analysis assuming that the flaring is linear and consider two values $\xi = 0.01$ and $\xi = 0.02$.

Once h_R , h_{σ_R} , h_{σ_ϕ} , $h_{\sigma_{Rz}}$ and ξ are fixed, we only need to set h_z to measure F_z^{est} , F_R^{est} and Γ^{est} , using Eqs. (10)-(12). Then, we can adjust $V_{h,\odot}$ and β_h of our mass model to match *simultaneously* F_z^{est} , F_R^{est} and Γ^{est} . The local circular velocity corresponding to the halo, $V_{h,\odot}$, is not permitted to be larger than 174 km s^{-1} to guarantee that $V_{c,0} < 250 \text{ km s}^{-1}$. We comment that the local surface density is uniquely determined by F_z and Γ (see Equation 4). Indeed, two models having the same F_z and Γ should have the same surface density even if they have different F_R . Still, it is useful to fit also F_R^{est} to reduce uncertainties in the parameters.

We find that the quality of the fits depends on the selected value for h_z ; the best fits are obtained when h_z lies between 0.64 kpc and 0.7 kpc. These values of h_z are consistent with the scale height derived in Bilir et al. (2008), Polido et al. (2013), Jia et al. (2014) and López-Corredoira et al. (2015). Other authors measure

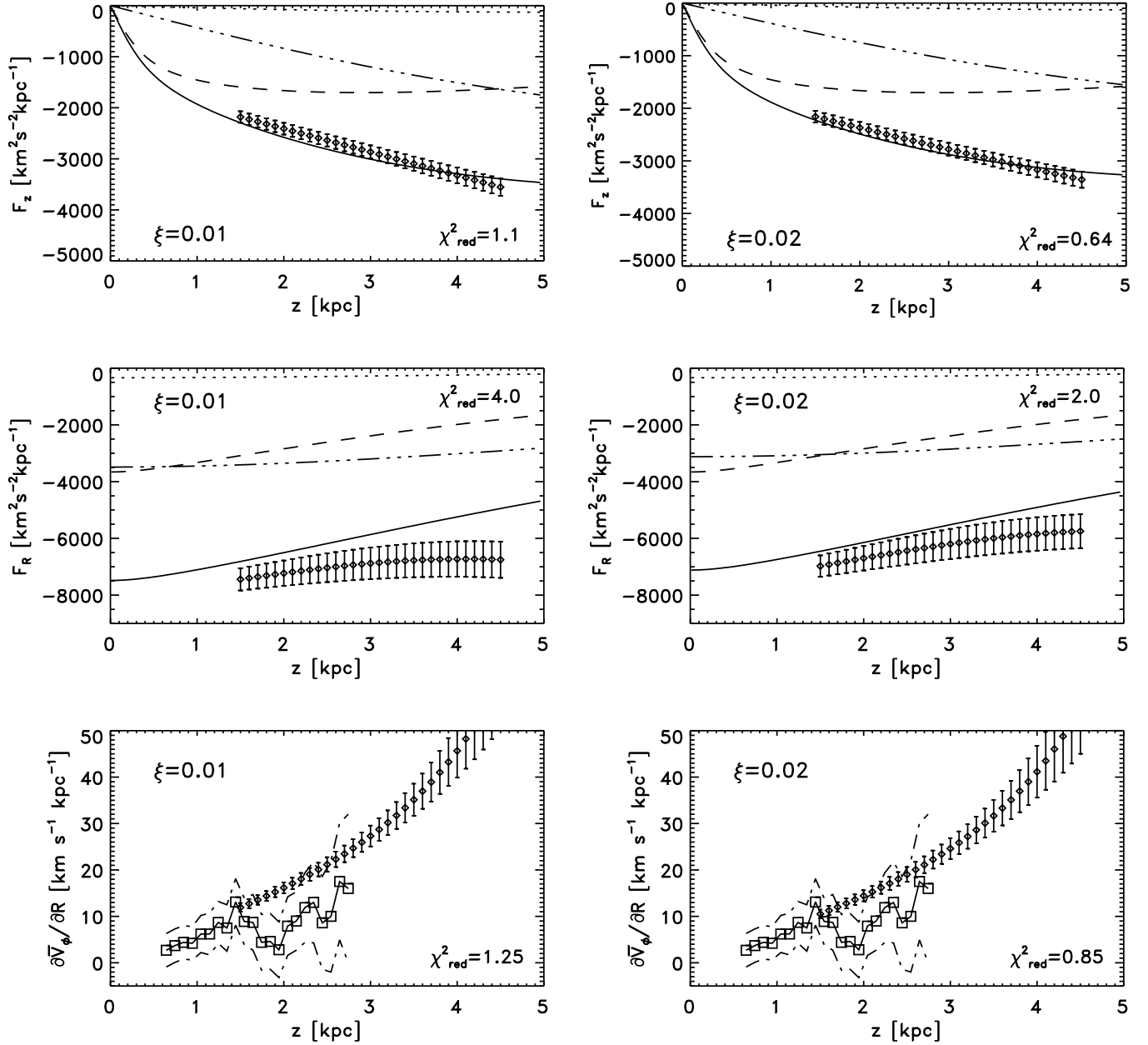


FIG. 9.— Vertical profiles of F_z , F_R and $\partial\bar{V}_\phi/\partial R$. In the left column, the solid lines indicate the profiles for a mass model with $V_h = 167$ km s^{-1} and $\beta_h = 0.35$. In the right column, solid curves are for a mass model with $V_h = 158$ km s^{-1} and $\beta_h = 0.32$. The contribution of the disk (dashed line), bulge (dotted line) and halo (triple dotted-dashed line) are also shown. The dots with error bars indicate the dynamical measurements for $\xi = 0.01$ (left column) and $\xi = 0.02$ (right column). The dynamical estimates for F_z , F_R and $\partial\bar{V}_\phi/\partial R$ were calculated using Equations (10)-(12). In Equation (12) we used the values of Γ of the corresponding mass model described above. In the bottom panels, the squares represent the observed value and the dash-dot lines the 1σ confidence interval. For the tracer thick disk population, we have used $h_R = 3.6$ kpc and $h_z = 0.68$ kpc. The χ^2_{red} -value is given in each panel.

scaleheights up to 1.0 kpc (for a compilation, see Table 1 in Jia et al. 2014).

Figure 9 shows our best fits for $h_z = 0.68$ kpc. For σ_{Rz}^2 , we have used the fit given in Equation (23). Instead of Γ , we show $\partial\bar{V}_\phi/\partial R$ as derived using Equation (12) and compare it with the observed measurements. The reduced chi-square, χ^2_{red} , are quoted at a corner in each panel.

For $h_z = 0.68$ kpc and $\xi = 0.01$ (and using our fiducial values of the geometrical parameters), we find

$V_{h,\odot} = 167 \pm 2$ km s^{-1} and $\beta_h = 0.35 \pm 0.10$ (thus $\rho_0 = 0.0135 \pm 0.002 M_\odot \text{pc}^{-3}$). For the same h_z but for $\xi = 0.02$, we get $V_{h,\odot} = 158 \pm 2$ km s^{-1} and $\beta_h = 0.32 \pm 0.10$ (hence $\rho_0 = 0.012 \pm 0.002 M_\odot \text{pc}^{-3}$). These models have local circular velocities at the mid-plane of ~ 240 km s^{-1} , and small values for Γ_0 (between -500 $\text{km}^2\text{s}^{-2}\text{kpc}^{-1}$ and 100 $\text{km}^2\text{s}^{-2}\text{kpc}^{-1}$), which are consistent with the values derived in §3.4 using the Oort constants.

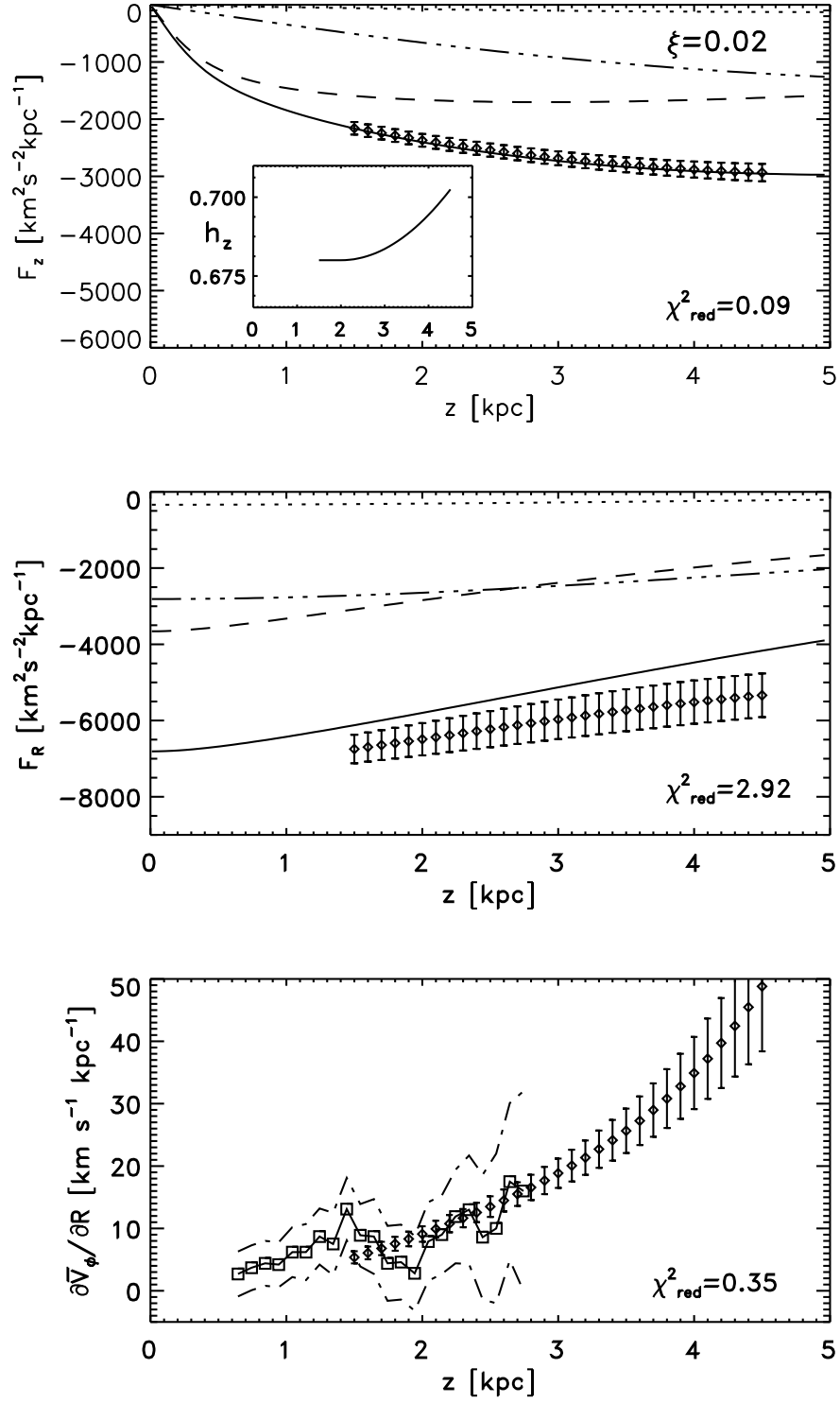


FIG. 10.— Same as Figure 9 but for a mass model with $V_{h,\odot} = 150 \text{ km s}^{-1}$ and $\beta_h = 0$ (implying that $V_{c,0} = 234 \text{ km s}^{-1}$, $\Gamma_0 = -2400 \text{ km}^2 \text{s}^{-2} \text{kpc}^{-1}$ and $\rho_0 = 0.0064 M_\odot \text{pc}^{-3}$). The scaleheight depends slightly on z , as it is shown in the inset plot at the top panel.

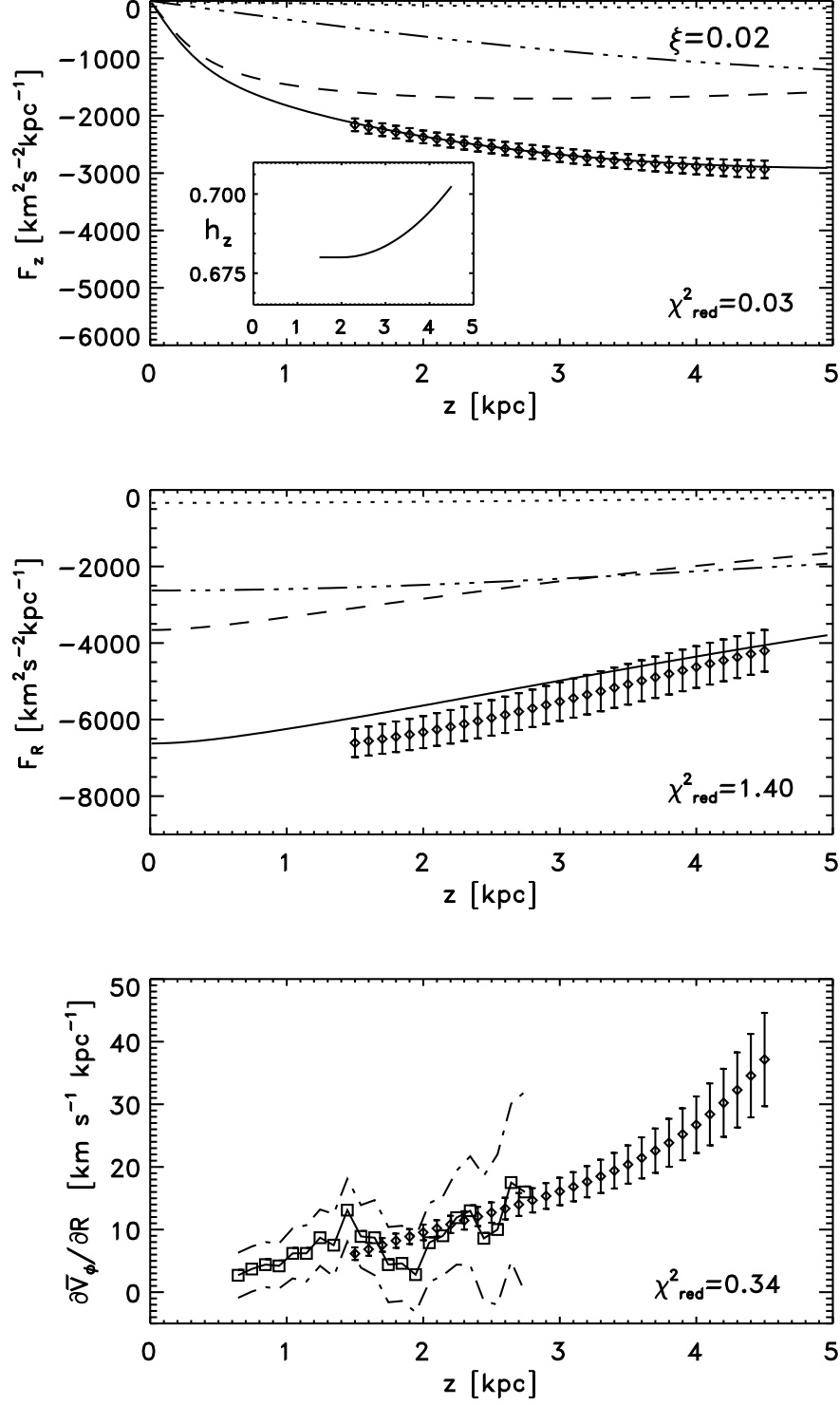


FIG. 11.— Same as Figure 9 but now for a thick disk with a scalelength h_{σ_R} that increases with z , from $h_{\sigma_R} = 4$ kpc at $z = 1.5$ kpc to $h_{\sigma_R} = 6.5$ kpc at $z = 4$ kpc. The solid lines represent the profiles for a mass model with $V_{h,\odot} = 145$ km s⁻¹ and $\beta_h = 0.05$, resulting in $V_{c,0} = 231$ km s⁻¹, $\Gamma_0 = -2100$ km² s⁻² kpc⁻¹ and $\rho_0 = 0.0066 M_\odot \text{pc}^{-3}$.

The goodness of the fits to F_z^{est} is statistically similar for $\xi = 0.01$ and $\xi = 0.02$. The curves F_z^{est} vs z are linear in both cases, while the vertical profile F_z of the best-fitting mass models present some curvature. If the thick disk is not strictly exponential along z (e.g., §4.2 and Carollo et al. 2010), but h_z increases slightly from $z = 1.5$ kpc to $z = 4.5$ kpc, then F_z^{est} vs z is not longer linear but flattens. A small deviation from a strict vertical exponential profile provides a good fit to the z -component of the force (see below).

In §3.2, we showed that, when $\xi = 0$, the shape of F_R^{est} vs z is unphysical. However, for $\xi = 0.02$, the shape of F_R^{est} vs z appears reasonable (see Figure 9). Still, the model underestimates $|F_R|$ over the errors. It is worthwhile noticing that the slope of F_R in the mass models is essentially given by the baryonic disk because the contribution of the halo is almost flat. If we adopt a larger value for $V_{h,\odot}$, $|F_R|$ of the mass model increases but, since F_R^{est} depends implicitly on $V_{c,0}$ through the term \bar{V}_ϕ^2/R (see Equations 11 and 24), a larger $V_{h,\odot}$ also implies a higher $|F_R^{\text{est}}|$. Thus, the convergence $F_R \rightarrow F_R^{\text{est}}$ by changing $V_{h,\odot}$ is very slow. In fact, we need $V_{h,\odot} \simeq 190$ km s $^{-1}$ and, thereby $V_{c,0} \simeq 260$ km s $^{-1}$ to account for F_R^{est} . Since this value for $V_{c,0}$ is not very plausible, the lack of a mass model able to fit F_R^{est} is telling us that either the selected geometrical parameters are not correct, the flaring of the disk is higher than we assumed or, more likely, the kinematical data are biased (or a combination).

The vertical profile for $\partial\bar{V}_\phi/\partial R$, derived using Equation (12), is compared with the observed values of this quantity by Moni Bidin et al. (2015). We see that although the values of χ_{red}^2 are close to 1, the estimated values of $\partial\bar{V}_\phi/\partial R$ systematically lie over the observed values, which is not very satisfactory.

Satisfactory fits to $\partial\bar{V}_\phi/\partial R$, can be achieved using a somewhat lower value for β_h . Figure 10 shows a mass model which was tailored to fit both F_z and $\partial\bar{V}_\phi/\partial R$. The mass model has $\rho_0 = 0.0064 M_\odot \text{pc}^{-3}$. In this fit, we have used a z -dependent vertical scale height to improve the F_z fit. We see that the F_R -fit is slightly worsened and, more importantly, the value of Γ_0 in this mass model is -2400 km 2 s $^{-2}$ kpc $^{-1}$, which is just outside the range derived using measurements of the Oort constants in §3.4.

If the assumption that $h_{\sigma_{ij}}$ are constant with z are relaxed, the F_R -fit can be improved. Our mock thick disk described in §4 suggests that all $h_{\sigma_{ij}}$ increase with z , particularly h_{σ_R} . For illustration, Figure 11 shows the case where h_{σ_R} increases from 4 kpc at $z = 1.5$ kpc to 6.5 kpc at $z = 4$ kpc in the following manner:

$$h_{\sigma_R}[\text{kpc}] = 4 + 0.4(z - 1.5)^2. \quad (35)$$

The halo parameters for this model are $V_{h,\odot} = 145 \pm 3$ km s $^{-1}$ and $\beta_h = 0.05 \pm 0.1$. In this model, the local DM density, ρ_0 , is $0.0066 \pm 0.0015 M_\odot \text{pc}^{-3}$. The value for χ_{red}^2 of the F_R -fit is a bit less ($\simeq 1.4$), but not fully satisfactory.

In order to explore the sensitivity of the fits to the adopted values of the geometrical parameters, we recalculated the best-fitting halo parameters using h_{σ_R} as given in Equation (35), but $h_{\sigma_\phi} = h_{\sigma_{Rz}} = 4.15$ kpc,

as derived by Hattori & Gilmore (2015) for h_{σ_z} . The best fitting parameters are $V_{h,\odot} = 142 \pm 3$ km s $^{-1}$ and $\beta_h = 0.13 \pm 0.1$, implying $\rho_0 = 0.0073 \pm 0.0015 M_\odot \text{pc}^{-3}$. The value of Γ_0 is -1730 km 2 s $^{-2}$ kpc $^{-1}$, which is reasonable.

The quoted errors in ρ_0 do not include uncertainties in the level of flattening of the dark halo, in the gas and stellar surface density, in the value of R_\odot , or associated with the assumption that the tracers are exponentially distributed in radius and height (see Hessman 2015 and McKee et al. 2015, for a recent discussion of these issues).

5.3. Discussion

In the previous subsection we found that acceptable fits to F_z^{est} , F_R^{est} and Γ^{est} are obtained for $h_z \simeq 0.68$ kpc and $h_R \gtrsim 3.6$ kpc. These models have local circular velocities of the halo, $V_{h,\odot}$, in the range 140-155 km s $^{-1}$ and the β_h parameter between 0 and 0.15. In all these models, $\rho_0 \gtrsim 0.0064 \pm 0.0015 M_\odot \text{pc}^{-3}$. Fits of the same quality can be achieved if both h_z and h_R are reduced simultaneously; for instance, taking $h_z = 0.64$ kpc and $h_R = 3.4$ kpc, we can find fits of the same quality, although a slightly larger ρ_0 is required.

While these values for h_z and h_R seem reasonable [e.g., de Jong et al. (2010) found $h_R = 4.1 \pm 0.4$ kpc and $h_z = 0.75 \pm 0.07$ kpc and Bilir et al. (2008) derived a height of $0.55 - 0.72$ kpc assuming $h_R = 3.5$ kpc; see also Polido et al. (2013) for similar values], recent studies with a larger cover in altitude and longitude suggest a shorter scalelength, $h_R \sim 2.3$ kpc, for the thick disk (Robin et al. 2014 and references therein). Therefore, it is relevant to consider models with a smaller value for h_R .

Figure 12 shows a case with $h_R = 2.5$ kpc, h_{σ_R} following Equation (35) and $h_{\sigma_\phi} = h_{\sigma_{Rz}} = 4.15$ kpc. The flaring parameter was also taken $\xi = 0.02$. The reduction in h_R leads to higher values for both $|F_z^{\text{est}}|$ and $|F_R^{\text{est}}|$, thus ρ_0 increases. If the fits to F_z^{est} and $\partial\bar{V}_\phi/\partial R$ are forced to be as good as in the previous cases, the F_R fit becomes poorer. In this case, the best-fitting halo parameters are $V_{h,\odot} = 155$ km s $^{-1}$ and $\beta_h = 0.05$ ($\rho_0 = 0.0076 M_\odot \text{pc}^{-3}$).

As already said in the previous Subsection, the local surface density is uniquely determined by F_z and Γ . In order to derive the local surface density, we only need to know F_z and Γ . Thus, a bad fit to F_R is not critical regarding the estimate the local volume density because the Poisson equation does not depend on F_R ; if the kinematical data is reliable, good fits to F_z and $\partial\bar{V}_\phi/\partial R$ would be enough to infer the local volume density of mass. Taken at face value, a mismatch between F_R^{est} and F_R in the model could be indicative that the halo is not spherical interior to R_\odot . Still, it turns out that the value of $V_{c,0}$ required to account for F_R^{est} , as derived for $h_R = 2.5$ kpc, is excessively large, even if the halo is prolate. This may indicate the kinematical data is contaminated by systematic uncertainties.

In conclusion, for $h_R \sim 2.5$ kpc, F_R^{est} cannot be fitted satisfactorily, unless $V_{c,0}$ is unusually large. Thus, we suggest that much of the offset between F_R^{est} and what models predict is caused by systematics in the data. If we fit simultaneously F_z^{est} and Γ^{est} , and ignore F_R^{est} (because it does not participate in the Poisson equation) then we obtain $\rho_0 = 0.0076 \pm 0.002 M_\odot \text{pc}^{-3}$ for $h_z \simeq 0.68$ kpc. As already said, a reduction of h_R results in a higher

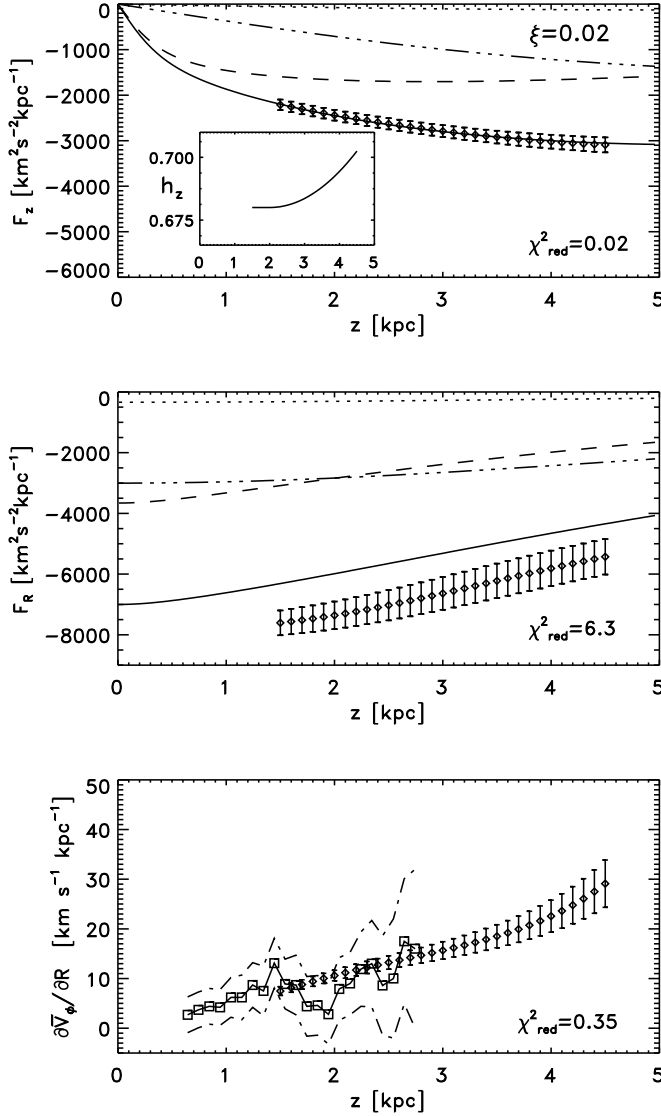


FIG. 12.— Vertical profiles of F_z^{est} , F_R^{est} and Γ^{est} for the following geometrical parameters: $h_R = 2.5$ kpc, h_{σ_R} as given in Equation (35), $h_{\sigma_\phi} = h_{\sigma_{Rz}} = 4.15$ kpc. The mass model has $V_{h,\odot} = 155$ km s^{-1} and $\beta_h = 0.05$. Thus, $V_{c,0} = 237$ km s^{-1} , $\Gamma_0 = -2080$ $\text{km}^2 \text{s}^{-2} \text{kpc}^{-1}$ and $\rho_0 = 0.0076 M_\odot \text{pc}^{-3}$.

value for ρ_0 because $|F_z^{\text{est}}|$ increases, whereas Γ^{est} is independent of h_R . Moni Bidin et al. (2012b) found that large values for h_R , typically $h_R \sim 4.7$ kpc, were required to recover the standard values for ρ_0 . This result is a consequence of their different assumptions; mainly their hypothesis that $h_R = h_\sigma$.

So far, we have assumed that the baryonic disk can be described by an exponential disk with a mass-weighted scale length, R_d , of 2.1 kpc. If R_d is larger, the baryonic mass in the disk turns to be smaller and hence more DM is required to account for the dynamics. Typically, ρ_0 increases by 20%, if we adopt $R_d = 3$ kpc instead of 2.1 kpc.

6. SUMMARY AND CONCLUSIONS

Having knowledge of the volume density $\nu(R_\odot, z)$ and vertical velocity for a vast number of some equilib-

rium tracer stars, the dynamical surface density can be measured at heights $|z| < 1.5$ kpc above the Galactic midplane, using the one-dimensional approximation, i.e. $S_{FR} \simeq 0$ and neglecting the σ_{Rz}^2 -tilt term in the Jeans equation (e.g., Kuijken & Gilmore 1989; Read 2014). At higher Galactic heights, the one-dimensional approximation may introduce bias (Siebert et al. 2008; Smith et al. 2009; Garbari et al. 2012; McKee et al. 2015). Bovy & Tremaine (2012) claimed that the assumption $S_{FR} \simeq 0$ provides a robust lower limit to the surface density at $|z| > 1.5$ kpc, as far as $\partial V_c / \partial R \simeq 0$ in the midplane. Using the sample of thick disk stars reported in Moni Bidin et al. (2012a), Bovy & Tremaine (2012) found that the mean halo density between $z = 1$ and $z = 4$ kpc is $0.0095 \pm 0.0015 M_\odot \text{pc}^{-3}$ for $h_R = 2$ kpc and $h_z = 0.7$ kpc or $0.007 \pm 0.001 M_\odot \text{pc}^{-3}$ for $h_R = 3.8$ kpc and $h_z = 0.9$ kpc.

Moni Bidin et al. (2015) have challenged the $S_{FR} \geq 0$ assumption of Bovy & Tremaine (2012) on the basis that it is not generally true that it holds for any Galactic potential. Moni Bidin et al. (2015) argue that this assumption is implicitly constraining the mass distribution and, thus, it is not adequate to derive ρ_0 . In order to release this hypothesis, Moni Bidin et al. (2015) moved beyond the one-dimensional approximation and, instead of assuming $S_{FR} \simeq 0$ (or, equivalently $\Gamma \simeq 0$), they used a dynamical measure of Γ as a function of z , which was derived from the kinematics of the same tracer population. The computation of Γ requires knowledge of \bar{V}_ϕ , which implicitly depends on the local circular velocity at the midplane, and $\partial \bar{V}_\phi / \partial R$, which is rather uncertain. Using this three-dimensional formalism, Moni Bidin et al. (2015) found that the density of DM at $|z| > 1.5$ kpc is $0 \pm 0.002 M_\odot \text{pc}^{-3}$ for $h_R = 2$ kpc and $h_z = 0.7$ kpc and $0.002 \pm 0.003 M_\odot \text{pc}^{-3}$ for $h_R = 3.6$ kpc and $h_z = 0.9$ kpc. These results are at variance with those derived by Bovy & Tremaine (2012). In order to fully understand this discrepancy, we investigated the robustness of both approaches in detail.

We have shown that the cMB estimator (after correcting it by a missed term in Moni Bidin et al. 2012b, 2015) is more sensitive to uncertainties in the geometrical parameters of the thick disk, particularly on h_σ , than the BT estimator. Therefore, accurate determinations of the dynamical surface density require good measures of the radial scalelengths of each of the components of the velocity dispersion tensor.

Using the Jeans equations and the current data of the kinematics of thick disk stars, we derived the vertical profiles of F_z , F_R and Γ . Assuming $V_{c,0} = 215$ km s^{-1} and $h_\sigma = 3.5$ kpc, we found that the kinematical estimates of F_R and Γ are biased towards large negative values. Possible causes are: poor model assumptions (e.g., neglecting the flare of the thick disk), uncertainties in the adopted values for $V_{c,0}$, \bar{V}_ϕ or $\partial \bar{V}_\phi / \partial R$, systematic overestimations of σ_R , σ_ϕ , or σ_{Rz} , or underestimations of the radial scalelengths of the components of the velocity dispersion tensor.

We have built simple but representative Galactic models consisting of the bulge, the baryonic disk and a DM component, having a local DM density as those inferred by the BT estimator and the cMB estimator (using $h_\sigma = 3.5$ kpc and $V_{c,0} = 215$ km s^{-1}). We have com-

pared F_z , F_R and Γ in these Galactic mass models with their corresponding estimates using the currently available kinematical data of the thick disk and found significant discrepancies between them. This implies that either the mass models do not describe correctly the underlying Galactic potential, or systematic errors and uncertain assumptions are affecting the dynamical estimates of F_z , F_R and Γ . We also stress the result that mass distributions with different local surface density may exhibit similar values of both F_z and F_R . To discriminate between these models, precise measurements of Γ_0 are required. Since the currently available kinematical data of thick disk stars are not good enough to provide a precise value of Γ_0 , we conclude that these data are not sufficient to constrain $\Sigma(z)$ without making further assumptions.

In order to examine the role and magnitude of the different systematics, we applied the BT and cMB estimators to estimate the surface density of a mock thick disk of tracer stars embedded in a fixed Milky Way-like gravitational potential, and compared with the exact input value. To do so, we prepared a thick disk population as close as we could to the assumptions behind the three-dimensional approach, namely, a thick disk following a rather homogeneous, doubly exponential distribution of stars in radius and height. However, our simulated thick disk has $h_{\sigma_{ij}}$ that depend strongly on z , whereas the cMB approach assumes that they are constant with z . Our analysis suggests that, even if $V_{c,0}$, \bar{V}_ϕ , $\partial\bar{V}_\phi/\partial R$ and all the mean geometrical parameters of the thick disk were accurately known, inaccuracies underpredict Γ by a

factor of 3 at $z = 3.5$ kpc above the disk. Still, the cMB formula, applied to our mock data, was able to recover the input surface density within the uncertainties.

Under the assumption that the DM halo is spherically symmetric interior to the radius $\sim 1.15R_\odot$, we have explored what configuration of parameters is more compatible with the current kinematic data of the thick disk. We have used a parametric mass model, consisting of the bulge, the baryonic disk and a dark halo. We have fit F_z^{est} , F_R^{est} and Γ^{est} with two free parameters; the contribution of the dark halo to the local circular velocity $V_{h,\odot}$ and the power-law exponent β_h . Acceptable fits are obtained if the thick disk is slightly flared and for the following geometrical parameters: $h_z \sim 0.7$ kpc, $h_R \gtrsim 3.5$ kpc, $h_R \gtrsim 4$ kpc, $h_{\sigma_\phi} \gtrsim 4$ kpc, and for a dark halo with $\rho_0 \gtrsim 0.0064 M_\odot \text{pc}^{-3}$. For smaller values of h_R , the estimated value for ρ_0 increases, but the fit to F_R worsens.

The currently available kinematical data of the thick disk stars up to 4 kpc above the Galactic midplane, may be also compatible with a flatten disk-like distribution of DM, having a DM density at $|z| > 1.5$ kpc as low as that derived in Moni Bidin et al. (2015). However, this model possibly has too large negative values of Γ_0 .

We thank the referee, Dr. C. Moni Bidin, for a very detailed report and constructive comments, which helped to improve the quality of the paper significantly. This work has been partly supported by CONACyT project 165584.

APPENDIX

A. ON THE SECOND-ORDER DERIVATIVES IN THE JEANS EQUATIONS

In §2.1, we used the Jeans equations to obtain the formulae for F_z , F_R and Γ as a function of the velocity dispersions and scalelengths of a tracer population. We considered that the tracer population is a flaring stellar disk, and assumed that the velocity dispersion components have exponential profiles along the R -direction. It is useful to derive F_z , F_R and Γ in a general form. We define the generalized geometrical factors, which depend on (R, z) , as:

$$\tilde{h}_z^{-1} \equiv -\frac{1}{\nu} \frac{\partial \nu}{\partial z}, \quad \tilde{h}_R^{-1} \equiv -\frac{1}{\nu} \frac{\partial \nu}{\partial R}, \quad H_R^{-2} \equiv \frac{1}{\nu} \frac{\partial^2 \nu}{\partial R^2}, \quad (\text{A1})$$

and

$$\tilde{h}_{\sigma_{ij}}^{-1} \equiv -\frac{1}{\sigma_{ij}^2} \frac{\partial \sigma_{ij}^2}{\partial R}, \quad H_{\sigma_{ij}}^{-2} \equiv \frac{1}{\sigma_{ij}^2} \frac{\partial^2 \sigma_{ij}^2}{\partial R^2}. \quad (\text{A2})$$

Equations (1) and (2) can be written as

$$F_z = \frac{\partial \sigma_z^2}{\partial z} - \frac{\sigma_z^2}{\tilde{h}_z} + \tilde{k}_0 \sigma_{Rz}^2, \quad (\text{A3})$$

with $\tilde{k}_0 \equiv R^{-1} - \tilde{h}_R^{-1} - \tilde{h}_{\sigma_{Rz}}^{-1}$ and

$$F_R = \tilde{k}_0' \sigma_R^2 - \frac{1}{R} (\sigma_\phi^2 + \bar{V}_\phi^2) + \frac{\partial \sigma_{Rz}^2}{\partial z} - \frac{\sigma_{Rz}^2}{\tilde{h}_z}, \quad (\text{A4})$$

with $\tilde{k}_0' \equiv R^{-1} - \tilde{h}_R^{-1} - \tilde{h}_{\sigma_R}^{-1}$. Finally, Γ is given by:

$$-\Gamma = K_1 \sigma_R^2 + \frac{\sigma_\phi^2}{\tilde{h}_{\sigma_\phi}} \pm K_2 R \frac{\sigma_{Rz}^2}{\tilde{h}_z} + \frac{\partial \sigma_{Rz}^2}{\partial z} + R \frac{\partial^2 \sigma_{Rz}^2}{\partial z \partial R} - \frac{\partial \bar{V}_\phi^2}{\partial R}, \quad (\text{A5})$$

where

$$K_1 = \left(\frac{1}{H_R^2} - \frac{1}{\tilde{h}_R^2} + \frac{1}{\tilde{h}_R \tilde{h}_{\sigma_R}} + \frac{1}{H_{\sigma_R}^2} \right) R - \frac{1}{\tilde{h}_R} - \frac{2}{\tilde{h}_{\sigma_R}}, \quad (\text{A6})$$

and

$$K_2 = \frac{1}{\tilde{h}_{\sigma_{Rz}}} - \frac{1}{R} - \frac{1}{\tilde{h}_R} + \frac{\tilde{h}_z}{\nu} \frac{\partial^2 \nu}{\partial z \partial R}. \quad (\text{A7})$$

The geometrical parameters \tilde{h}_z , \tilde{h}_R and $\tilde{h}_{\sigma_{ij}}$ are essentially local derivatives of ν and σ_{ij}^2 , which can be measured in the simulations at a generic point (R, z) . However, in §4.2, we computed Γ assuming that $H_R = \tilde{h}_R$ and $H_{\sigma_R} = \tilde{h}_{\sigma_R}$, which is only correct when ν and σ_R^2 have strict exponential profiles with R . In particular, if ν and $\sigma_{\sigma_R}^2$ have exponential profiles in the R -direction, then $H_R = \tilde{h}_R$, $H_{\sigma_R} = \tilde{h}_{\sigma_R}$, and hence

$$K_1 = \left(\frac{1}{\tilde{h}_R \tilde{h}_{\sigma_R}} + \frac{1}{\tilde{h}_{\sigma_R}^2} \right) R - \frac{1}{\tilde{h}_R} - \frac{2}{\tilde{h}_{\sigma_R}}, \quad (\text{A8})$$

and

$$K_2 = \frac{1}{\tilde{h}_{\sigma_{Rz}}} - \frac{1}{R}. \quad (\text{A9})$$

If ν and σ_R^2 are not exponential but follow a power-law along R , such as

$$\nu = \nu_{\odot}(z) \left(\frac{R_{\odot}}{R} \right)^{l_{\nu}}, \quad (\text{A10})$$

and

$$\sigma_R^2 = \sigma_{R,\odot}^2(z) \left(\frac{R_{\odot}}{R} \right)^{l_{\sigma}}, \quad (\text{A11})$$

we get

$$K_1 = [l_{\nu} + l_{\sigma}(1 + l_{\sigma})] \frac{1}{R} - \frac{1}{\tilde{h}_R} - \frac{2}{\tilde{h}_{\sigma_R}}, \quad (\text{A12})$$

and

$$K_2 = \frac{1}{\tilde{h}_{\sigma_{Rz}}} + \frac{l_{\nu} - 1}{R} - \frac{1}{\tilde{h}_R}. \quad (\text{A13})$$

In the simulations, it is very difficult to measure H_R and H_{σ_R} , particularly at high z . For instance, consider the R -profile of σ_R^2 . Between $R = 4$ kpc and $R = 12$ kpc, σ_R^2 vs R in a cut along $z = 3.5$ kpc, can be fitted equally well with an exponential profile with $\tilde{h}_{\sigma_R} = 30$ kpc than with a power-law profile with $l_{\sigma} = 0.25$. In the first case $H_{\sigma_R} = 30$ kpc, whereas in the second case $H_{\sigma_R} = 14.5$ kpc. This uncertainty in the second-order derivatives were not included in the analysis of §4.2.

B. MIYAMOTO-NAGAI DISK PLUS A SPHERICAL HALO

Consider an axisymmetric distribution of mass consisting of a Miyamoto & Nagai (1985) disk and a spherically-symmetric component. The gravitational potential is given by the sum of the contribution of the disk Φ_d plus the contribution of the spherical component Φ_{sph} . We define the corresponding circular velocities of the disk and spherical component (halo+bulge) as

$$V_{c,d}^2(R, z) \equiv R \frac{\partial \Phi_d}{\partial R}, \quad (\text{B1})$$

and

$$V_{c,sph}^2(R, z) \equiv R \frac{\partial \Phi_{sph}}{\partial R}. \quad (\text{B2})$$

Thus $V_c^2 = V_{c,d}^2 + V_{c,sph}^2$. We aim to compute how Γ varies with z at a given R .

After some simple algebraic manipulations, we find

$$\frac{\partial V_{c,sph}^2}{\partial R} = \frac{R}{r^2} \left(\frac{R^2 + 2z^2}{r} \frac{d\Phi_{sph}}{dr} + R^2 \frac{d^2 \Phi_{sph}}{dr^2} \right), \quad (\text{B3})$$

where $r^2 = R^2 + z^2$. In addition to the circular velocity $V_{c,sph}$, it is useful to define the circular velocity of a tilted orbit in the spherical potential,

$$V_{\text{tilt}}^2 \equiv r \frac{d\Phi_{sph}}{dr}. \quad (\text{B4})$$

Using this definition, we can rewrite

$$\frac{\partial V_{c,sph}^2}{\partial R} = \frac{2Rz^2}{r^4} V_{\text{tilt}}^2 + \frac{R^3}{r^3} \frac{dV_{\text{tilt}}^2}{dr} \quad (\text{B5})$$

or, equivalently,

$$\frac{\partial V_{c, sph}^2}{\partial R} = \frac{2R}{r^4} V_{\text{tilt}}^2 (z^2 + \beta R^2), \quad (\text{B6})$$

where

$$\beta(r) = \frac{d \ln V_{\text{tilt}}}{d \ln r}. \quad (\text{B7})$$

From Eq. (B6), we see that if $\beta \geq 0$ (a flat rotation curve corresponds to $\beta = 0$), then $\partial V_{c, sph}^2 / \partial R \geq 0$ at any z , implying that the contribution of the spherical component to S_{F_R} is positive or zero ($S_{F_R}^{sph} \geq 0$). Moreover, in order for $\partial V_{c, sph}^2 / \partial R$ to be negative, we require that $\beta < 0$ and $z^2 < -\beta R^2$. Hence, at a fixed R , one can always find a height $z_{\text{turn}} = \sqrt{-\beta} R$ at which $\partial V_{c, sph}^2 / \partial R > 0$ for any $z \geq z_{\text{turn}}$. Since $\beta \geq -0.5$ (the case $\beta = -0.5$ corresponds to the Keplerian decay), we have that $z_{\text{turn}} \leq R/\sqrt{2}$.

For the Miyamoto & Nagai disk with mass M_d and scale parameters a and b , the radial derivative of the circular velocity is

$$\frac{\partial V_{c, d}^2}{\partial R} = \frac{2GM_d R}{d^3} \left[1 - \frac{3}{2} \frac{R^2}{d^2} \right], \quad (\text{B8})$$

where $d^2(R, z) \equiv R^2 + (a + \sqrt{z^2 + b^2})^2$.

REFERENCES

- Aalseth, C. E., Barbeau, P. S., Colaresi, J., et al. 2013, *PhRvD*, 88, 012002
- Aartsen, M. G., Abraham, K., Ackermann, M., et al. 2015, *arXiv:1505.07259*, EPJC
- Agnes, R., Ahmed, Z., Anderson, A. J., et al. 2013, *PhRvL*, 111, 251301
- Angloher, G., Bauer, M., Bavykina, I., et al. 2012, EPJC, 72, 1971
- Bahcall, J. N., Flynn, C., & Gould, A. 1992, *ApJ*, 389, 234
- Bernabei, R., Belli, P., Cappella, F., et al. 2010, EPJC, 67, 39
- Bienaymé, O., Famaey, B., Siebert, A., et al. 2014, *A&A*, 571, 92
- Bilir, S., Cabrera-Lavers, A., Karaali, S., et al. 2008, *PASA*, 25, 69
- Bovy, J., & Rix, H.-W. 2013, *ApJ*, 779, 115
- Bovy, J., Rix, H.-W., Hogg, D. W., et al. 2012a, *ApJ*, 755, 115
- Bovy, J., Allende Prieto, C., Beers, T. C., et al. 2012b, *ApJ*, 759, 131
- Branham, R. L. 2010, *MNRAS*, 409, 1269
- Carollo, D., Beers, T. C., Chiba, M., et al. 2010, *ApJ*, 712, 692
- Casetti-Dinescu, D. I., Girard, T. M., Korchagin, V. I., & van Altena, W. F. 2011, *ApJ*, 728, 7
- Catena, R., & Ullio, P. 2010, *JCAP*, 08, 004
- Feast, M., & Whitelock, P. 1997, *MNRAS*, 291, 683
- Flynn, C., Sommer-Larsen, J., & Christensen, P. R. 1996, *MNRAS*, 281, 1027
- Fuchs, B., Dettbarn, C., Rix, H.-W., et al. 2009, *AJ*, 137, 4149
- Garbari, S., Liu, C., Read, J. I., & Lake, G. 2012, *MNRAS*, 425, 1445
- Hattori, K., & Gilmore, G. 2015, *MNRAS*, 454, 649
- Hessman, F. V. 2015, *A&A*, 579, 123
- Holmberg, J., & Flynn, C. 2000, *MNRAS*, 313, 209
- Iocco, F., Pato, M., Bertone, G., & Jetzer, P. 2011, *JCAP*, 11, 029
- Ivezić, Z., Sesar, B., Jurić, M., et al. 2008, *ApJ*, 684, 287
- Jia, Y., Du, C., Wu, Z. et al. 2014, *MNRAS*, 441, 503
- Jurić, M., Ivezić, Z., Brooks, A., et al. 2008, *ApJ*, 673, 864
- Kuijken, K., & Gilmore, G. 1989, *MNRAS*, 239, 571
- Lewis, J. R., & Freeman, K. C. 1989, *AJ*, 97, 139
- López-Corredoira, M., & Molgó, J. 2014, *A&A*, 567, 106
- Mateu, C., Vivas, A. K., Downes, J. J., & Briceño, C. 2011, *RMxAA*, 40, 245
- McKee, C. F., Parravano, A., & Hollenbach, D. J. 2015, *ApJ*, 814, 13
- McMillan, P. 2011, *MNRAS*, 414, 2446
- Mignard, F. 2000, *A&A*, 354, 522
- Minchev, I., Martig, M., Streich, D., et al. 2015, *ApJ*, 804, L9
- Miyamoto, M., & Nagai, R. 1975, *PASJ*, 27, 533
- Moni Bidin, C., Carraro, G., Méndez, R. A., & van Altena, W. F. 2010, *ApJ*, 724, L122
- Moni Bidin, C., Carraro, G., & Méndez, R. A. 2012a, *ApJ*, 747, 101
- Moni Bidin, C., Carraro, G., Méndez, R. A., & Smith, R. 2012b, *ApJ*, 751, 30
- Moni Bidin, C., Smith, R., Carraro, G., Méndez, R. A., & Moyano, M. 2015, *A&A*, 573, 91
- Nesti, F., & Salucci, P. 2013, *JCAP*, 1307, 016
- Olling, R. P., & Dehnen, W. 2003, *ApJ*, 599, 275
- Pillepich, A., Kuhlen, M., Guedes, J., & Madau, P. 2014, *ApJ*, 784, 161
- Piffi, T., Binney, J., McMillan, P. J., et al. 2014, *MNRAS*, 445, 3133
- Piffi, T., Penoyre, Z., & Binney, J. 2015, *MNRAS*, 451, 639
- Polido, P., Jablonski, F., & Lépine, J. 2013, *ApJ*, 778, 32
- Read, J. I. 2014, *JPhG*, 41, 063101
- Read, J. I., Lake, G., Agertz, O., & Debattista, V. P. 2008, *MNRAS*, 389, 1041
- Read, J. I., Mayer, L., Brooks, A. M., Governato, F., & Lake, G. 2009, *MNRAS*, 397, 44
- Robin, A. C., Reylé, C., Fliri, J., et al. 2014, *A&A*, 569, 13
- Ruchti, G. R., Read, J. I., Feltzing, S., Pipino, A., & Bensby, T. 2014, *MNRAS*, 444, 515
- Salucci, P., Nesti, F., Gentile, G., & Frigerio Martins, C. 2010, *A&A*, 523, 83
- Sanders, J. 2012, *MNRAS*, 425, 2228
- Siebert, A., Bienaymé, O., Binney, J., et al. 2008, *MNRAS*, 391, 793
- Siegel, M. H., Majewski, S. R., Reid, I. N., & Thompson, I. B. 2002, *ApJ*, 578, 151
- Smith, M. C., Evans, N. W., & An, J. H. 2009, *ApJ*, 698, 1110
- Sofue, Y. 2009, *PASJ*, 61, 153
- Vera-Ciro, C., & Helmi, A. 2013, *ApJ*, 773, L4
- Wang, W., Han, J., Cooper, A., et al. 2015, *MNRAS*, 453, 377
- Weber, M., & de Boer, W. 2010, *A&A*, 509, 25
- Widrow, L. M., Pym, B., & Dubinski, J. 2008, *ApJ*, 679, 1239
- Wolfire, M. G., McKee, C. F., Hollenbach, D., & Tielens, A. G. G. M. 2003, *ApJ*, 587, 278
- York, D. G., Adelman, J., Anderson, Jr. J. E., et al. 2000, *AJ*, 120, 1579
- Yuan, F.-T., Zhu, Z., Kong, D.-L. 2008, *ChJAA*, 8, 714
- Zhang, L., Rix, H.-W., van de Ven, G., et al. 2013, *ApJ*, 772, 108